



저작자표시-비영리-변경금지 2.0 대한민국

이용자는 아래의 조건을 따르는 경우에 한하여 자유롭게

- 이 저작물을 복제, 배포, 전송, 전시, 공연 및 방송할 수 있습니다.

다음과 같은 조건을 따라야 합니다:



저작자표시. 귀하는 원저작자를 표시하여야 합니다.



비영리. 귀하는 이 저작물을 영리 목적으로 이용할 수 없습니다.

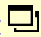


변경금지. 귀하는 이 저작물을 개작, 변형 또는 가공할 수 없습니다.

- 귀하는, 이 저작물의 재이용이나 배포의 경우, 이 저작물에 적용된 이용허락조건을 명확하게 나타내어야 합니다.
- 저작권자로부터 별도의 허가를 받으면 이러한 조건들은 적용되지 않습니다.

저작권법에 따른 이용자의 권리는 위의 내용에 의하여 영향을 받지 않습니다.

이것은 [이용허락규약\(Legal Code\)](#)을 이해하기 쉽게 요약한 것입니다.

[Disclaimer](#) 

의학박사 학위논문

Application of Stromal Vascular
Fractions from Fat Tissues to
Improve Dendritic Cell-Mediated
Immune Responses

지방조직 유래 기질혈관분획을 활용한
수지상세포 매개 면역반응 향상

2020년 8월

서울대학교 대학원
의과학과 의과학전공
이재원

A thesis of the Degree of Doctor of Philosophy

Application of Stromal Vascular
Fractions from Fat Tissues to
Improve Dendritic Cell–Mediated
Immune Responses

지방조직 유래 기질혈관분획을 활용한
수지상세포 매개 면역반응 향상

August 2020

Major in Biomedical Sciences
Department of Biomedical Sciences
Seoul National University Graduate School
Jae–Won Lee

1. Abstract

Application of Stromal Vascular Fractions from Fat Tissues to Improve Dendritic Cell–Mediated Immune Responses

Jae–Won Lee

Major in Biomedical Sciences
Department of Biomedical Sciences
The Graduate School
Seoul National University

Introduction: Dendritic cell (DC) is the most potent antigen presenting cell. The DCs capture antigens from tumors or invading pathogens and delivery them to naive T cells in the lymph node, thereby priming an adaptive immune response. Based on the potency of DCs as professional antigen presenting cells, DCs have been applied to cancer immunotherapy. However, clinical outcomes have not been satisfactory. To improve the efficacy of DC–based therapy, stromal cells collected from fat tissues were applied as structural frames that support the

functionality of DCs for priming and boosting antigen-specific T cell responses *in vivo*.

Methods: To acquire the stromal cells, stromal vascular fractions (SVFs) were isolated from visceral and subcutaneous fat tissues of C57B/L6 mice via enzymatic digestion. SVF spheroids (SPHs) were generated by culturing SVFs *in vitro* for 6~10 days and seeding them in a spheroid-forming film. To assess differential gene expression in SVF and SPH, transcriptome and quantitative real-time RT-PCR were performed. DCs were prepared from bone marrow (BM) cells in Rag2 $-/-$ mice. BMDCs were loaded with Fe₃O₄-ZnO core-shell nanoparticles (FZ-NPs) and ZnO-binding peptide (ZBP)-ovalbumin (OVA) complex and activated by lipopolysaccharides. *In vivo* organogenesis by SPHs and a mature DC mixture was examined after the renal subcapsular transplantation. *In vivo* structure was observed by confocal image and histological image. Antigen-specific immune responses were assessed after the immunization of mice with SPH and DC complexes, followed by staining with MHC-tetramer specific to OVA-peptide. The anti-tumor effect of immunization with SPH and DC complexes was also examined in mice bearing transplanted B16 melanoma expressing OVA.

Results: This study found that cultured SVFs consisted of cells phenotypically and functionally similar to LN stromal cells. SVF SPHs generated vessel-like structures *in vitro* and *in vivo*. Moreover, SVF SPHs expressed various chemokines and attracted DCs *in vitro*. In addition, mature DCs co-cultured with SVFs showed enhanced activation and survival. Transplantation of SVF SPHs complexed with mature DCs also recruited T cells

into the injection site in the kidney subcapsule. Immunization with SVF SPHs and OVA antigen-loaded DCs significantly improved antigen-specific T cell responses when compared with the administration of SVF SPHs or DCs alone. Moreover, the treatment of SVF SPHs and DC complexes showed significantly enhanced tumor suppression when compared with control groups.

Conclusion: Taken together, cultured SVFs can be used as a functional frame mimicking LN stromal cells and can support the functionality of DCs, leading to enhanced antigen-specific T cell responses and an anti-tumor effect. Therefore, the present study suggests that SVFs isolated from fat tissues could be applied as promising cellular resources to improve DC-mediated immune response.

Keywords: Stromal vascular fraction, Dendritic cell, Immunotherapy, Tertiary lymphoid structure, Lymph node stromal cells

Student number: 2014-25071

2. Contents

1. Abstract	1
2. Contents	4
3. List of Tables and Figures	5
4. List of Abbreviations	7
5. Introduction	9
6. Materials & methods	14
7. Results	24
8. Discussion	68
9. References	75
10. 국문 초록	84

3. List of Tables and Figures

Table. 1. Primers for qPCR	19
Figure 1. Schematic Illustration of Strategy to Improve Dendritic Cell-Mediated Immune Responses Using Stromal Vascular Fractions	13
Figure 2. Characterization of Stromal Vascular Fractions (SVFs)	28
Figure 3. Characterization of CD45 ⁺ Hematopoietic Cells in Cultured SVFs	30
Figure 4. Characterization of CD45 ⁻ Non-Hematopoietic Cells in Cultured SVFs	32
Figure 5. The Expression of LN FRC Markers Expressed on PDPN ⁺ CD31 ⁻ Cells of the Cultured SVFs	34
Figure 6. The Gene Expression of Chemokines in SVFs in Context-Dependent Manner	36
Figure 7. The Spheroid Form of SVFs Can Generate Vessel-Like Structures	40
Figure 8. The Vessel-Like Structures Formed from SVF Spheroids Could Act as Migration Routes of Immune Cells	42
Figure 9. Comparison of SVFs and Spheroid Form of SVFs	44

Figure 10. Gene Expression Analysis of SVF Spheroids	49
Figure 11. SVF Spheroids Can Recruit Dendritic Cells	50
Figure 12. <i>In vivo</i> Organogenesis by Transplantation of SVF Spheroids and Dendritic Cells into the Kidney Subcapsular Space	52
Figure 13. Analysis of Cell Population of the Transplants	54
Figure 14. Phenotypes of Infiltrated T Cells in Transplants	56
Figure 15. The Transcriptomic Analysis of Co-Cultured SVFs and DCs	60
Figure 16. SVFs Regulate Activation and Survival of Immune Cells	62
Figure 17. Characteristics of Fe ₃ O ₄ -ZnO Core-Shell Nanoparticle	64
Figure 18. The Administration of SPH with DCs Enhances the Antigen-Specific Immune Response <i>in vivo</i>	65
Figure 19. Anti-Tumor Effect of SVF SPH with DCs	68
Figure 20. Summary and Proposed Mechanism	76

4. List of Abbreviations

Actb: β -actin

ATMC: adipose tissue-derived mesenchymal cell

BEC: blood endothelial cell

BMDC: bone marrow-derived dendritic cell

cDNA: complementary DNA

DAPI: 4',6-diamidino-2-phenylindole

DC: dendritic cell

FRC: fibroblastic reticular cell

FZ-NP: Fe₃O₄-ZnO core-shell nanoparticle

H&E: hematoxylin and eosin

HEV: high endothelial venule

ICAM-1: intracellular adhesion molecule -1

LEC: lymphatic endothelial cell

LN: lymph node

LNSC: lymph node stromal cell

LPS: lipopolysaccharide

LTi: lymphoid tissue inducer cell

LTo: lymphoid tissue organizer cell

LT β R: lymphotoxin β receptor

mDC: mature BMDC

MHC: major histocompatibility complex

NP: nanoparticle

OVA: ovalbumin

PDPN: podoplanin

PECAM-1: platelet endothelial cell adhesion molecule-1

qPCR: quantitative polymerase chain reaction

SC: stromal cell

SPH: spheroid

SVF: stromal vascular fraction

TEM: transmission electron microscopy

TLS: tertiary lymphoid structure

TME: tumor microenvironment

VCAM-1: vascular cell adhesion molecule -1

VEGFR3: vascular endothelial growth factor receptor

ZBP: ZnO-binding peptide

5. Introduction

Dendritic cell (DC) is a potent inducer of innate and adaptive immunity.¹ DCs derived from CD34⁺ hematopoietic stem cells in the bone marrow spread throughout and monitor the whole body in the blood, peripheral tissues, and lymphoid organs.^{1,2} DCs can capture, process, deliver, and present the antigens to naive T cells in the lymph nodes.^{3,4} Not only can DCs present the fragment of exogenous antigens upon major histocompatibility complex (MHC) type II to CD4⁺ T cells, but can also cross-present intracellular antigens via MHC type I to CD8⁺ T cells.⁵ In addition to antigens from protein, the C-type lectin receptors on the surface (i.e. DEC205, DC-SIGN) allow DCs to recognize the glycoproteins or nucleoproteins from dying cells and cross-present them to T cells.^{6,7} Once immature DCs bearing the antigens are activated by various stimuli, mature (activated) DCs migrate from peripheral tissues to the T cell areas in the draining lymph node and subsequently prime T cells with the upregulated MHC II and co-stimulatory molecules (i.e. CD40, CD80, CD86) and by secreting cytokines (i.e., interleukin (IL)-12 and interferon (IFN) α).^{3,8-11} In cancer immunology, DCs contribute to provoking an anti-tumor immune response and re-activate T cells by capturing, presenting the tumor-associated antigens including cross-presentation, and expressing co-stimulatory molecules and immuno-stimulatory cytokines in the tumor site or tumor-draining lymph node.^{12,13} Furthermore, DCs produce the chemokines which attract T cells, resulting in T cell infiltration in the tumor microenvironment (TME).¹⁴ Therefore, the stimulatory role of DCs in T cell

responses is particularly important in anti-tumor immunity.

Based on such an essential role in anti-tumor response and their safety in clinical application, DCs were utilized as cancer immunotherapy.¹⁵ The first clinical trial was performed in the 1990s; however, clinical response rates have been less than 15% for the last two decades.^{16,17} To improve the poor clinical response rate, DC-therapy has several hurdles to overcome. Firstly, DCs must migrate to draining LNs and get the chance to encounter T cells in order to initiate adaptive immune responses because the larger amount of injected DCs generally relates to a positive prognosis.^{18,19} However, multiple reports have claimed that only about 4–5% of DCs could migrate to draining LNs and most of them remained at the injection site.^{20–22} Moreover, TME suppresses the immune response provoked against tumors not only at the tumor site^{23,24} but in the tumor-draining LNs^{25–27}, limiting the original capability of intact DC-based immunotherapy. Therefore, to augment the antigen-specific immune response and restore the full potential of DC-based therapy, it is compulsory to utilize DCs remaining at the injection site and to evade the effects of TME.

DCs encounter T cells in particular locations called "specialized compartments of lymphoid organs" for appropriate T-cell priming and activation.²⁸ These places consist of different CD45⁻ non-hematopoietic stromal cells including fibroblastic and endothelial stromal cells. The stromal cells are normally distinguished by the expression of the fibroblast marker podoplanin (PDPN, gp38) and endothelial marker CD31 (platelet endothelial cell adhesion molecule-1, PECAM-1).²⁹ PDPN⁺CD31⁻ fibroblastic reticular cells (FRCs) provide the structural support,

organizing the conduit system which transports soluble antigens, and form a three-dimensional cell-to-cell network where immune cells migrate.³⁰ The production of chemokine CCL19 and CCL21 by FRCs attracts CCR7⁺ T cells and DCs, resulting in increasing T cell interactions with DCs, promoting the maturation of DCs and presenting antigens by DCs.³¹ FRCs also control the homeostasis of T cells and DCs via secretion of IL-7 and IL-15.^{28,32} Additionally, PDPN expressed on FRCs promote DC motility.²¹ Recently, it was reported that FRC-derived IL-6 enhanced the survival and metabolism of CD8⁺ T cells and led to generate tissue-resident memory T cells via chromatin remodeling.^{33,34} PDPN⁺CD31⁺ lymphatic endothelial cells (LECs) compose the afferent and efferent lymphatic vessels, mediating the movement of leukocytes and lymph.³⁵ LECs control the subset of T cells.^{36,37} PDPN⁻CD31⁺ blood endothelial cells (BECs) form blood vessels and high endothelial venules (HEVs). BECs are involved in the transmigration of lymphocytes from the bloodstream.^{28,29,35,37} Therefore, owing to these structural and functional supportive roles of the stromal cells, DCs in the DC-based immunotherapy might require such support from stromal cells to fully induce an anti-tumoral T cell response. Nevertheless, it is very difficult to obtain functional stromal cells from lymphoid organs because the stromal cells reside in less than 5% of the tissue.³⁸ The amount is almost too small to use, making it nearly impossible to use them for therapy.

Fat tissue is usually considered as a redundant part of the body. However, most of the LNs are surrounded by adipose tissue, which plays a role as a source of stromal precursors during embryonic development or the expansion of the adult

lymph node.³⁹ A study revealed that pre-adipocytes from adult fat tissues differentiated into a variety of LN stromal cells.⁴⁰ Another study showed that adipose tissue-derived mesenchymal cells (ATMC) cultured with embryonic thymus or mesenteric LN generated LN structures containing T and B cell zones.⁴¹ Indeed, some fat tissues include multiple lymphoid structures, which protect the cavities from inflammation and infection, called “milky spots” in omentum⁴² or “fat-associated lymphoid clusters” in visceral fat.⁴³ These studies implicate that adipose tissues can serve as a source of LN stromal cells. As a way to acquire those types of cells, stromal vascular fractions (SVFs) isolated from fat tissues include multifarious cells such as lymphocytes, adipocyte precursors, adipocyte-derived stromal cells, fibroblast, endothelial cells and pericytes.⁴⁴ SVFs are cultivated to remove lymphocytes, and then adherent and heterogenous stromal-shaped cells can be obtained.⁴⁵

Based on the aforementioned reasons, the motivation of the current study is that the cultured SVFs can be an alternative of LN stromal cells and SVFs with DCs can enhance the immune response via *in situ* induction of immune clusters (Fig. 1). Here, the present study reported that SVF spheroids cultured with DCs could provide structural and functional support to DCs and attracted more T cells, resulting in a sufficiently improved antigen-specific immune response against tumors.

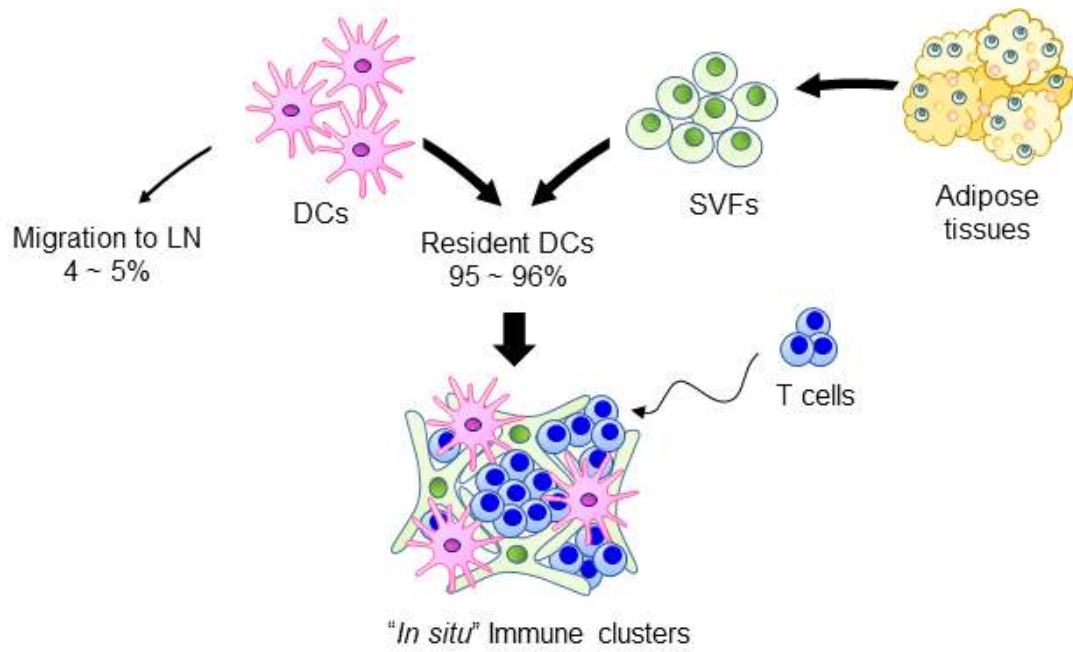


Figure 1. Schematic Illustration of Strategy to Improve Dendritic Cell-Mediated Immune Responses Using Stromal Vascular Fractions.

6. Materials & methods

Mice. C57BL/6 wildtype mice (Koatech, Seoul, Korea) and C57BL/10NAGCSnAi-(KO) Rag2 (H-2^b) mice (Taconic Biosciences, NY, USA) were housed and maintained in the specific pathogen-free facility at the Seoul National University College of Medicine. All mice were male and used at 6–12 weeks of age. All mice experiments were approved by the Seoul National University Institutional Animal Care and Use Committee (IACUC). (IACUC Number: SNU-150115-2-7, SNU-160212-2-7, SNU-171123-4-7).

Isolation of stromal vascular fractions (SVF) and spheroid cultures. Visceral and subcutaneous fat tissues were collected and finely chopped, and then the tissues were incubated with 0.8 mg/mL Collagenase IV and 100 μ g/mL DNaseI in sterile Hank's balanced salt solution (Intron, Seoul, Korea) including 3% bovine serum albumin (BSA) (MP biomedical, CA, USA), 1.0 mM CaCl₂ (Sigma-Aldrich, MO, USA) and 0.8 mM MgCl₂ (Sigma-Aldrich, MO, USA) for 1 h at 37°C on the shaker at 170 rpm. After centrifugation at 500 g for 3 min, the supernatant was discarded and the pellet was collected, followed by incubation for the indicated days in Dulbecco's Modified Eagle Medium (Welgene, Daegu, Korea) containing 10% fetal bovine serum (Gibco, MA, USA) and 1% penicillin/streptomycin (Gibco, MA, USA) (Fig. 2a). For spheroids, SVFs cultured for 6–10 days were trypsinized and counted. Cultured SVFs were seeded in a spheroid film (Incyto, Cheonan, Korea). 361 (19 x 19) SVF spheroids were generated in a spheroid film. Following incubation for more than 2 days, the spheroid form of SVFs was used for

the experiments.

Preparation of Fe_3O_4 -ZnO core-shell nanoparticles. Fe_3O_4 -ZnO core-shell nanoparticles (FZ-NPs) of 10.5 nm size were supplied by Prof. Young Keun Kim's laboratory at Korea University. The FZ-NPs were synthesized via a modified nano-emulsion method proposed in a previous report, although it was slightly modified in this study.^{46,47} First, for the synthesis of the Fe_3O_4 core, 0.1766 g of iron (III) acetylacetonate (0.5 mmol), 0.6468 g of 1,2-hexadecandiol (2.5 mmol), 0.7530g of poly(ethylene glycol)-block-poly(propylene glycol)-block-poly(ethylene glycol) (PEO-PPO-PEO) were dissolved in 15 mL of octyl ether at room temperature. The mixture was gradually heated to 120°C under vacuum condition, and then rapidly heated to 300°C for refluxing under Ar condition. After 1 h of refluxing, the black-colored solution was slowly cooled to room temperature. To form the ZnO shell, 0.2636 g of zinc acetylacetonate (1.0 mmol), 0.6468 g of 1,2-hexadecanediol (2.5 mmol), and 5 mL of octyl ether were added to the solution containing the Fe_3O_4 core. The mixed solution was heated to 80°C at a constant heating rate of 1°C/min and homogenized at 80°C for 2 h under Ar condition. After refluxing the solution for 1 h at 300°C, the products were precipitated by ethanol and washed at least five times using ultrasonication and centrifugation.

Characterization of Fe_3O_4 -ZnO core-shell nanoparticles. The morphologies and microstructures of the FZ-NPs were analyzed by transmission electron microscopy (TEM) (FEI, Tecnai F20 G2) at an accelerating voltage of 200 kV. Detailed dark-field and elemental-mapping images were obtained by analytical TEM (FEI, Talos F200X) at 200 kV. The samples for the TEM ex-

periments were prepared via washing in absolute ethanol. The samples were then dropped onto the TEM grid. The sizes of the samples were measured using the TEM images, and they followed a Gaussian distribution.

Production of recombinant ZnO-binding peptide (ZBP) – ovalbumin (OVA) proteins. To produce recombinant ZnO-binding OVA protein, genomic DNA of B16MO5 cell lines were first extracted using DNeasy Blood & Tissue Kits (Qiagen, Hilden, Germany) according to the manufacturer's instruction. Extracted DNA was PCR-amplified (Forward primer: 5' -TTT GAA TTC ATG GGC TCC ATC GGT GCA-3' , Reverse primer: 5' -AAA CTC GAG AGG GGA AAC ACA TCT GCC-3' , EcoRI and XhoI restriction sites underlined) and cloned into the pET23d-ZBP vector encoding 3xZBP
(BamHI-RPHRKGGDARPHRKGGDARPHRKGGDA-EcoRI).⁴⁶ The cloned vector pET23d-ZBPOVA was then transformed into E. coli, the HIT Competent BL21 strain (RBCBioscience, New Taipei City, Taiwan), according to the manufacturer's instructions. ZnO-binding OVA protein ZBPOVA was then purified with the protocol adapted from previously described methods.^{48,49} Briefly, isopropylthiogalactoside (IPTG; 0.1 mM) induced E. coli culture was lysed with an ice-cold buffer (300 mM NaCl and 50 mM phosphate at pH of 8.0) supplemented with lysozyme (1 mg/mL) and a protease inhibitor cocktail for 30 min and then further lysed by sonication. The lysate was then centrifuged and the collected supernatant was filtered and column-purified using AKTastart (GEHealthcare, IL, USA) and HisTrap™ FF (GEHealthcare, IL, USA). The protein was dialyzed in PBS 4°C overnight. Endotoxin was removed from the

purified protein using Triton X-114 as previously described.⁵⁰ Endotoxin contamination of the purified protein was determined using the Pierce LAL Chromogenic Endotoxin Quantification Kit (Thermo Fisher Scientific, MA, USA) according to the manufacturer's instruction. The purified ZBPOVA protein was quantified with SDS-PAGE and stored in -80°C until further use.

BMDC isolation, antigen delivery and maturation. Bone marrow (BM) was isolated and differentiated to DCs as previously described.⁵¹ In brief, BMs of Rag2 knock-out mice were isolated and incubated in Iscove's modified Eagle medium (IMDM) (Gibco, MA, USA) supplemented with 10% FBS, 1.5 ng/mL recombinant mouse GM-CSF (PeproTech, NJ, USA) and 1.5 ng/mL mouse IL-4 (PeproTech, NJ, USA), 1% penicillin/streptomycin, 50 $\mu\text{g/mL}$ gentamicin (Gibco, MA, USA), 2 mM L-glutamine (Gibco, MA, USA), and 50 nM β -mercaptoethanol (Gibco, MA, USA). Immature DCs were used following incubation for 6-8 days. The medium was replaced every other day. For intracellular antigen delivery to immature DCs, Fe_3O_4 -ZnO core-shell nanoparticles (FZ-NP) were used.⁴⁶ 100 μg FZ-NPs were washed by PBS three times and then FZ-NPs were incubated with 20 μg ZBP-OVA for 1 h at room temperature to bind to one another. Following FZ-NPs with ZBP-OVA (NP-OVA) were washed by IMDM three times, 1×10^6 DCs were incubated with NP-OVA for 1 h at 37°C . For maturation, DCs were treated with 1 $\mu\text{g/mL}$ lipopolysaccharides (LPS) for 16-18 h. Mature DCs by LPS were washed by IMDM three times before experiments.

Flow cytometric analysis and antibodies. The cells were blocked with a super-block solution including 10% goat serum (Thermo Fisher Scientific, MA, USA), 10% rat serum (Thermo Fisher

Scientific, MA, USA), 10% mouse serum (Sigma–Aldrich, MO, USA), and 10 $\mu\text{g}/\text{mL}$ of anti–CD16/CD32 (2.4G2) antibody (BD Pharmingen, NJ, USA) followed by surface staining for 30min on ice with APC/Cy7–conjugated anti–CD45, BV405–conjugated anti–CD11c, alexa488–conjugated anti–CD11c, APC–conjugated anti–B220, PE–conjugated anti–CD11b, APC–conjugated anti–PDPN, FITC–conjugated anti– ICAM–1, PE/Cy7–conjugated anti–CD31, PE–conjugated anti–LT β R, FITC–conjugated anti–VCAM–1, PE–conjugated anti–CD140 α , PerCP/Cy5.5–conjugated anti–CD44, PE/Cy7–conjugated anti–CD86, APC–conjugated anti–I–Ab, BV605–conjugated anti–Ki67 and PE–conjugated anti–DC–SIGN (Biolegend, CA, USA), PE–conjugated anti–CD3, BV421–conjugated anti–CD3, PerCP–conjugated anti–CD4, FITC–conjugated anti–CD8, APC–conjugated anti–Gr–1, BV605–conjugated anti–CD62L, FITC–conjugated anti–I–Ab and PE–conjugated anti–CD40 (BD Pharmingen, NJ, USA), PE/Cy7–conjugated anti–CD4, eFlour 450–conjugated anti–CD3, PE/Cy7–conjugated anti–F4/80, and APC–conjugated anti–CD80 (eBioscience, CA, USA). Live cells were distinct by staining with Zombi Aqua (Biolegend, CA, USA) or 7–amino–actinomycin D (7–AAD) (BD Pharmingen, NJ, USA). The cells were measured by LSRFortessa X–20 flow cytometer, BD LSRII flow cytometer (BD Pharmingen, NJ, USA), and CytoFLEX S (Beckman Coulter, CA, USA). The data was analyzed by FlowJo software (Tree Star, Ashland, OR, USA).

Renal Subcapsular Transplantation. The transplantation into the kidney subcapsule of SVF spheroids or DCs was performed as previously depicted.⁵² In brief, after anesthetizing the mouse and removing the flank fur, the skin was incised with disinfection and

the kidney was externalized. The graft was slowly inserted by using the threaded plunger (Hamilton, NV, USA), following the surface capsule on the kidney which was torn by 30-gauge needle (BD Pharmingen, NJ, USA). The scar was marked by a high temperature cautery (Bovie medical corporation, NY, USA) to seal. The kidney was returned into the body and the skin was sutured.

Quantitative PCR. The RNA extraction was performed by Trizol reagent (Invitrogen, CA, USA) following the standard protocols. Complementary DNA (cDNA) was sequentially synthesized by reverse transcript premix kit (Intron, Seoul, Korea). To confirm whether SVFs can secrete the principle chemokines of LN stromal cells, the mRNA expression was measured by quantitative PCR (qPCR), which was measured using the SYBR Green master mix (Life Technologies, CA, USA) and CFX Real Time PCR Detection System (Bio-Rad Laboratories, CA, USA). Each sample was examined in duplicate. Relative mRNA expression was calculated based on the value of β -actin (*Actb*). The primers are summarized in Table 1.

Table 1. Primers for qPCR.

Gene	5' -Foward Primer-3'	5' -Reverse Primer-3'	Base Pairs
<i>CCL19</i>	CCTGGGAACATCGTGAAAGC	TAGTGTGGTGAACACAACAGC	81
<i>CCL21</i>	GTGATGGAGGGGGTCAGGA	GGGATGGGACAGCCTAAACT	109
<i>CXCL13</i>	GGCCACGGTATTCTGGAAGC	GGGCGTAACTTGAATCCGATCTA	108
<i>CXCL12</i>	CATCAGTGACGGTAAACCAG	CACAGTTTGGAGTGTTGAGG	116
<i>Actb</i>	TGTTACCAACTGGGACGACATG	GGGGTGTTGAAGGTCTCAAAC	165

mRNA Sequencing. To characterize the gene expression of the SVFs day 0 and 8 and SVF spheroids, CD45⁻ population was sorted from SVFs at day 0 and 8 by using anti-CD45 microbeads and magnetic cell separation (MACS; Miltenyi Biotec, Bergisch Gladbach, Germany), followed by total RNA isolation. RNA quality was measured by Agilent 2100 bioanalyzer using the RNA 6000 Nano Chip (Agilent Technologies, Amstelveen, Netherlands), and RNA quantification was measured using the ND-2000 Spectrophotometer (Thermo Fisher Scientific, MA, USA). The libraries were generated from total RNA by using the SMARTer Stranded RNA-Seq Kit (Clontech Laboratories, CA, USA). Polyadenylated mRNA was specifically isolated by using the Poly(A) RNA Selection Kit (LEXOGEN, Vienna, Austria), followed by cDNA synthesis, shearing for fragmentation, and amplification by PCR sequentially. The mean fragment size was measured by the Agilent 2100 bioanalyzer and quantification was evaluated by the StepOne Real-Time PCR System (Life Technologies, CA, USA). The libraries were sequenced on paired-end 100-bp reads by HiSeq 2500 (Illumina, CA, USA). The sequenced data was mapped using TopHat.⁵³ Data was analyzed by ExDEGA (E-biogen, Seoul, Korea) and visualized by Prism 8 (GraphPad, CA, USA).

Enzyme-linked immune sorbent assay (ELISA). The translational expression of CCL21 and osteopontin in cell-culture supernatants was measured by ELSIA kits purchased from Research And Diagnostic Systems (MN, USA) and Lifespan Biosciences (WA, USA), respectively, according to the manufacturer's instructions.

Chemotaxis assay. To confirm the chemo-attractant ability of SVF spheroids, the chemotaxis assay was performed by using a μ -Slide Chemotaxis kit (Cat#80326; Ibidi, Grafelfing, Germany) following the manufacturer's description. 1.5 mg/mL of Type I Collagen solution (Corning, NY, USA) was injected in the observation area. SVF spheroids in the media or media alone were injected to the left space and splenocyte was inserted into the right space. The live cell imaging was taken during incubation for 24 h by FV1000 (Olympus corporation, Tokyo, Japan).

Co-culture SVFs with DCs or splenocytes. For the co-culture, the 24-well plates were prepared with 1×10^6 /well DCs alone, 1×10^6 /well splenocytes alone, 2×10^4 /well cultured SVFs with 1×10^6 /well mature DCs, or 1×10^6 /well splenocytes. After incubation for the indicated time, the cells were analyzed by flow cytometry.

***In vitro* and *in vivo* imaging.** SVFs during *in vitro* culture were observed by microscope (Olympus corporation, Tokyo, Japan) and VisiView software (Visitron systems, Puchheim, Germany). For immunofluorescence staining, cells cultured in collagen type 1 were fixed with 4% paraformaldehyde and incubated for 20 min at room temperature. After fixation, the fixed cells were permeabilized by 0.1% Triton X-100 for 10 min. For preventing non-specific binding, the samples were blocked with 1% BSA and incubated for 1 h at room temperature. Primary antibodies with 1% BSA, anti-LYVE1, and anti-CD31 (Abcam, Cambridge, UK) were filled into the well-plate and incubated for 2 h. After washing with 1X PBS three times, a mixture of Alexa Fluor conjugated goat anti-rabbit and -mouse secondary antibody,

rhodamine-phalloidin and 4',6-diamidino-2-phenylindole (Thermo Fisher Scientific, MA, US) were filled in the well-plate and incubated for 2 h. To confirm the structure resulted from *in vivo* kidney subcapsular transplantation, the graft was collected 2 weeks after the operation and was embedded with frozen section media (Leica Biosystems, IL, USA) and rapidly frozen in liquid nitrogen. The samples were cryo-sectioned to 5-6 μ m thick and stored at -80°C until the time of the experiments. For histological analysis, the cyro-sectioned segments were stained with hematoxylin and eosin (H&E) as in the earlier description.⁵⁴ For confocal imaging, the sectioned samples were fixed in 4% paraformaldehyde and stained with FITC-labeled anti-CD3, FITC-labeled anti-CD8 (BD Pharmingen, NJ, USA), alexa647-labeled anti-CD31, alexa594-labeled anti-PDPN, alexa647-labeled anti-CD11c, Alexa 647-labeled anti-CD4 (Biolegend, CA, USA), alexa 594-labeled anti-VEGFR3 (Bioss Antibodies, MA, USA), and 4',6-diamidino-2-phenylindole (DAPI; Thermo Fisher Scientific, MA, USA). Confocal images were taken by FV3000 (Olympus corporation, Tokyo, Japan) and analyzed by IMARIS version 9.3 (Bitplane, Zurich, Switzerland).

Assessment of antigen-specific immune response. To examine whether SVF spheroids plus DCs can effectively induce an antigen-specific immune response, the combinations (1×10^6 DCs/mouse or 361 of SVF spheroids/mouse or both) were transplanted into the kidney subcapsule of each mouse once every other week, 2 times in total. DCs were pulsed with NP-OVA and the same amount of NP-OVA was inserted into the SVF spheroid alone-transplanted group. 5 weeks after the first immunization, splenocytes isolated from each mouse were

incubated with OVA 257–264 peptide and OVA 339–323 peptide (InvivoGen, CA, USA), presented by H-2K^b major histocompatibility complex (MHC) class I and I-A^b MHC class II, respectively, to proliferate OVA-specific T cells. After incubation for 24 h, the cells were stained with anti-MHC tetramers for 30 min at 4°C, and then surface staining was performed for an additional 30 min, followed by flow cytometric analysis. APC-labeled tetramer SIINFEKL-H-2K^b and PE-labeled tetramer AAHAEINEA-I-A^b were kindly provided by the National Institutes of Health Tetramer Core Facility in the USA.

Tumor inoculation and anti-tumor effect test. For tumor inoculation, OVA-expressing melanoma B16MO5 (5x10⁴ cells/mouse) were injected into the left flank of mice. After 7 d, each combination (1x10⁶ DCs/mouse, 361 of SVF spheroids/mouse) was inserted under the kidney capsule three times at weekly intervals. Each group included five mice. To examine the anti-tumor effect, the tumor size and survival rate were assessed. The tumor was measured every 2–3 days. The tumor volume (mm³) was calculated as 1/2 x [(short diameter) x (long diameter)²]. Each mouse was considered dead when the tumor size grew to more than 2000 mm³.

Statistical analysis. The data was analyzed by GraphPad Prism software for statistical analysis. RNA-seq analysis was performed by ExDEGA version 2.5.

7. Results

1. Characterization of Cells in Stromal Vascular Fractions from Fat Tissues

SVFs were isolated from fat tissues through enzyme digestion (Fig. 2a) and were cultured for 6 days. The isolated cells contained relatively small (FSC < 250 K) and round-shaped cells on day 0 and were increasingly replaced with relatively larger (FSC > 250 K) and elongated cells over time (Fig. 2b–d). The frequency of low FSC (< 250 K) cells decreased from 83.88% on day 0 to 24.92% on day 6, while the frequency of high FSC (> 250 K) cells increased from 16.12% on day 0 to 75.08% on day 6. To confirm such alternation in cellularity more accurately, the cultured SVFs were analyzed by flow cytometry. The CD45⁺ hematopoietic cell population reduced from 23.4% to 5.94%, while the CD45⁻ non-hematopoietic cell population increased from 76.0% to 93.7% (Fig. 2e, f). Given that CD45⁺ hematopoietic cells are small, round-shaped, and short-lived *ex vivo* compared to CD45⁻ non-hematopoietic cells and that the CD45⁻ non-hematopoietic cell population grew both in number and size in cultured SVFs on day 6, low FSC cells on day 0 might include the CD45⁺ hematopoietic cells and CD45⁻ precursors, and high FSC cells on day 6 might contain the CD45⁻ adherent cells and CD45⁺ myeloid cells like DCs and macrophages which live relatively longer than lymphocytes. To further elucidate which cell types were present during the shift of cellularity, the cells were stained with specific pan markers

and then analyzed. As expected, the frequency of lymphocytes including CD4⁺ T cells, CD8⁺ T cells, and B220⁺ B cells quickly decreased within 5 days (Fig. 3a–c), while the frequency of CD11c⁺ DCs was retained until day 10 (Fig. 3d). Other myeloid cells such as CD11b⁺ F4/80⁺ macrophages and Gr-1⁺ neutrophils decreased in number in a time-dependent manner (Fig. 3e, f).

When the CD45⁻ non-hematopoietic cells were analyzed with stromal cell markers, PDPN and CD31, the population divided into a pattern that strongly resembled that of LN stromal cells (Fig. 4a). The frequency of PDPN⁺CD31⁻ FRC-like cells dramatically increased after 5 days and remained as the most abundant group during incubation, regardless of subculture (Fig. 4b). The frequency of PDPN⁻CD31⁺ BEC-like cells moderately increased from 4% on day 0 to 7% on day 5 but thereafter contracted and remained under 2% on day 10 and after subculture (Fig. 4c). The frequency of PDPN⁺CD31⁺ LEC-like cells had marginally increased until day 10 but decreased following subculture (Fig. 4d). The frequency of the PDPN⁻CD31⁻ double negative (DN)-population was initially more than 80% on day 0, but dramatically reduced after day 5 and remained under 20%. The ratio at which DN cells decreased was consistent with the ratio at which the rest increased. This might possibly indicate that FRC-, LEC-, and BEC-like cells might have been differentiated from the DN population, and not newly generated within each population.

The most abundant cell population, FRC-like cells were then further analyzed to see if they were phenotypically similar to LN FRCs. PDPN⁺CD31⁻ FRC-like cells highly expressed the

principle markers of FRC including lymphotoxin β receptor (LT β R), CD140 α (also known as platelet-derived growth factor α), vascular cell adhesion molecule-1 (VCAM-1), and intracellular adhesion molecule-1 (ICAM-1) (Fig. 5).²⁹ Consistent with the expansion of FRC-like cells during culture (Fig. 4b), the expression of all markers increased on day 5. Although the number of cell passages might have affected the expression level of those markers, it was clear that the phenotype of FRC-like cells was similar to that of LN FRCs.

In addition to expression markers, LN FRCs are functionally characterized by their expression of chemokines such as *ccl19*, *ccl21*, *cxcl13*, and *cxcl12* in response to various stimuli.²⁸⁻³⁰ To demonstrate whether cultured SVFs are also functionally related to FRCs, the mRNA expression of each chemokine in cultured SVFs was measured by quantitative PCR following stimulation via TLR3-agonist (PolyI:C), TLR7-agonist (Imiquimod), or LT β R ligands (anti-LT β R, LIGHT) for 24 h (Fig. 6a). All of the gene expressions significantly increased in response to PolyI:C, Imiquimod, and anti-LT β R, except for LIGHT. Therefore, in infection and inflammation status, SVFs might release chemokine to attract immune cells and provide an environment for cellular interaction. One of the major functions of LN stromal cells is to keep a structural network within the tissue in order to facilitate cellular interaction such as DCs and T cells and regulate adaptive immune response. To mimic such a niche, cultured SVFs were made into spheroids (SVF SPHs), a kind of 3-dimensional culture, to create a dense environment like LN to enhance the interactions between cells. The mRNA expressions of *ccl19*, *ccl21*, and *cxcl13* in SVF SPHs significantly increased

compared to those in 2D-cultured SVFs (Fig. 6b). Indeed, the amount of CCL21 secreted from SVF SPHs (516 pg/mL) was 12-fold greater than that of CCL21 secreted from 2D-cultured SVFs (41.1 pg/mL) (Fig. 6c). The results indicated that cultured SVFs can express the typical LN stromal-derived chemokines in context-dependent manner. Taken together, cultured SVFs isolated from fat tissues were composed of cells which phenotypically and functionally resembled LN stromal cells.

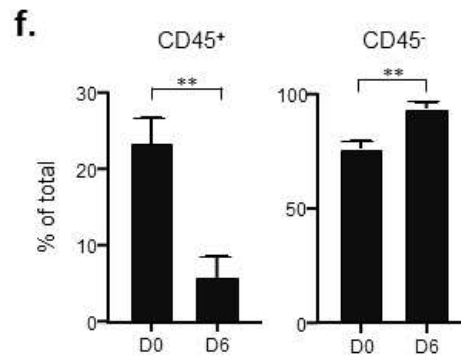
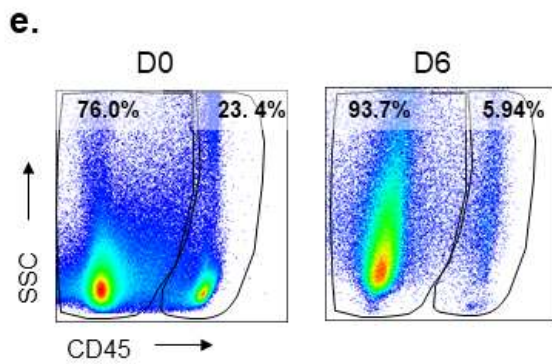
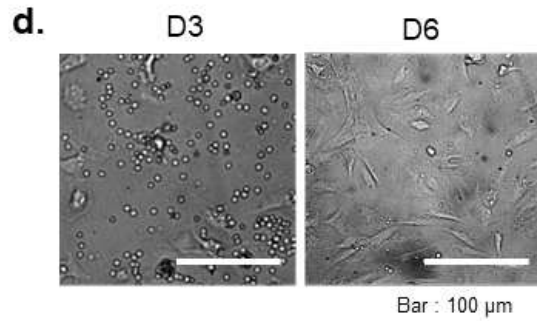
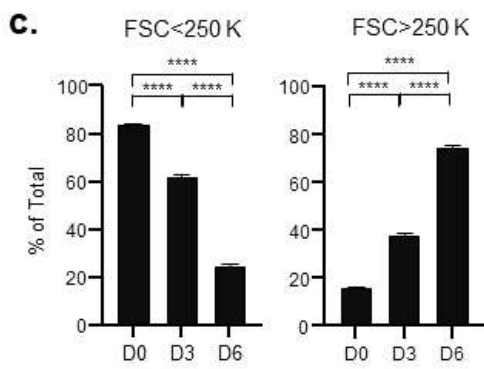
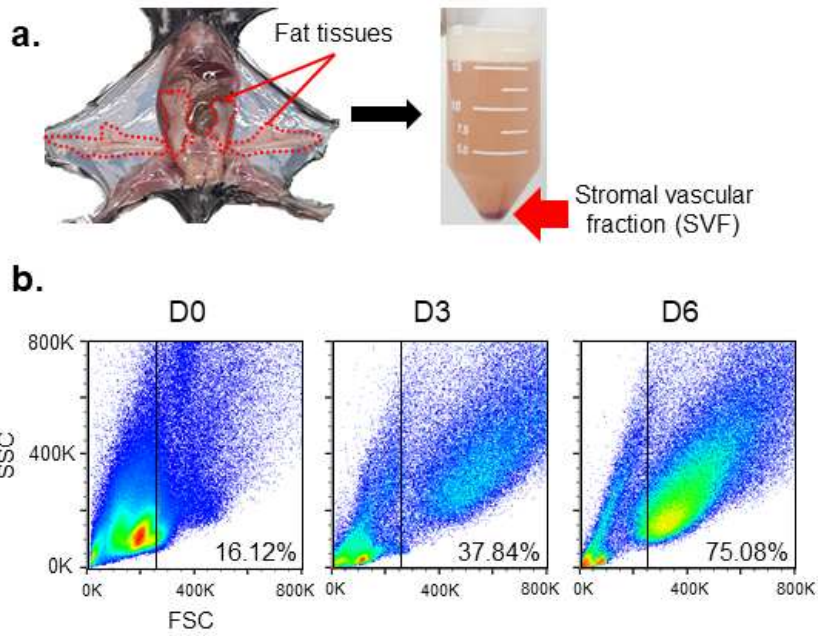


Figure 2. Characterization of Stromal Vascular Fractions (SVFs).

a, Extraction of SVFs from fat tissues. Visceral fat tissues used in the extraction were visualized with red dotted lines (left). The extracted SVFs after centrifugation were denoted with the red arrow (right). **b,** Representative flow cytometric images of the cell size on each of the days (day 0(D0), day 3 (D3), day 6(D6)) by forward scatter (FSC) and side scatter(SSC). **c,** Quantification of FSC<250 K cells (left) and FSC>250 K cells (right) (n=3 on the indicated day) **** $p<0.0001$ (ANOVA). **d,** Microscopic images of the cultured SVFs on day 3 and day 6. Scale bar: 100 μm . **e,** Gating strategy for flow cytometry of hematopoietic (CD45⁺) and non-hematopoietic cells (CD45⁻) of the cultured SVFs on day 0 and day 6. **f,** Quantification of CD45⁻ cells (left) and CD45⁺ cells (right) (n=3 on the indicated day) ** $p=0.0029$ on day 0, ** $p=0.0023$ on day 6 (two-tailed student' s t-test)

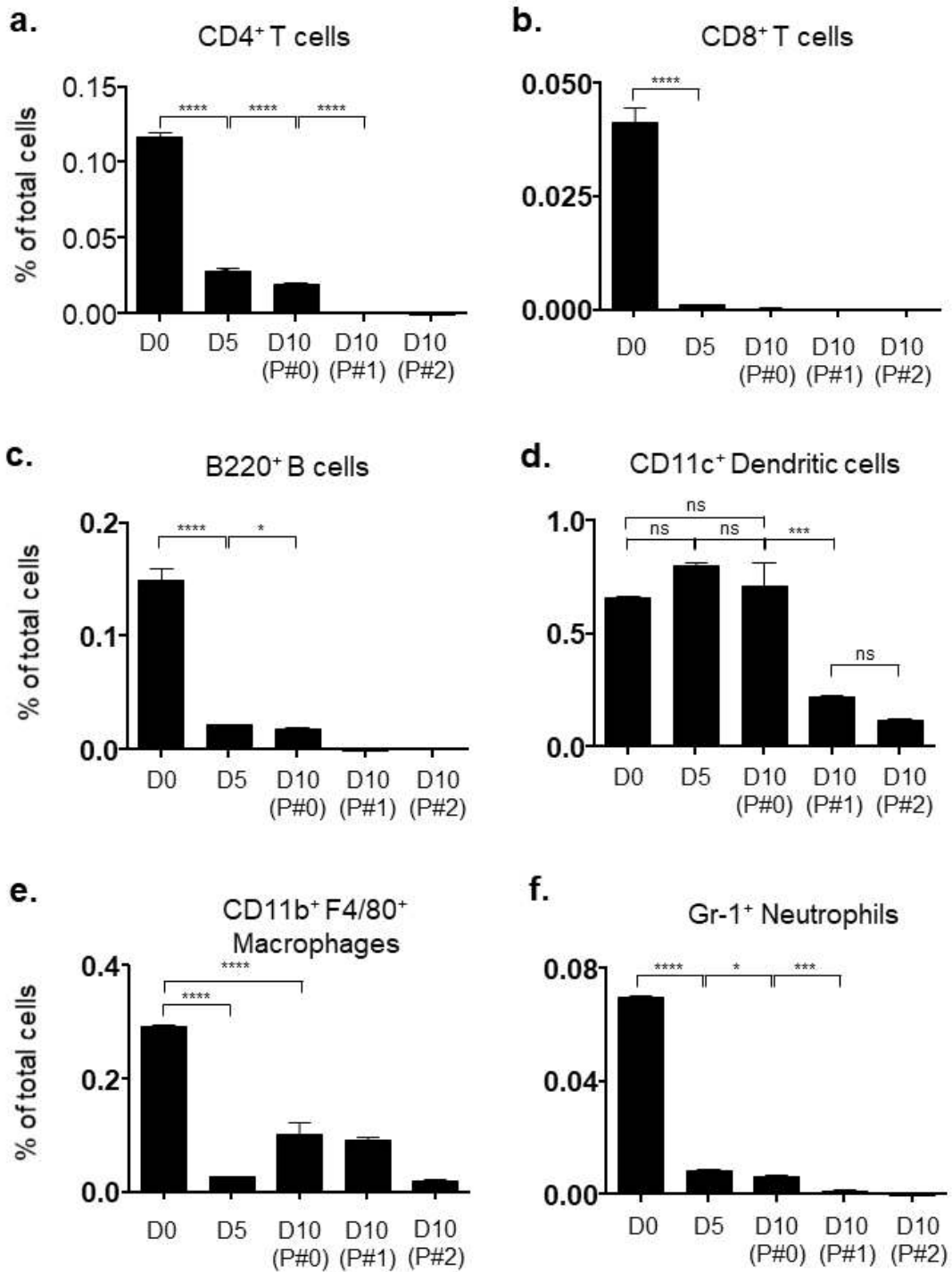


Figure 3. Characterization of CD45⁺ Hematopoietic Cells in Cultured SVFs. Flow cytometry measurement of total a, CD4⁺ T cells, b, CD8⁺ T cells, c, B cells, d, dendritic cells, e, macrophages, f, neutrophils on day 0 (D0), day 5 (D5), day 10 (D10) and day 10 before (passage 0 (P#0)) and after subculture (passage 1 (P#1), passage 2 (P#2)) (n=3 on the indicated day and passage) **** $p < 0.0001$, *** $p < 0.0002$, ** $p < 0.0021$, * $p < 0.0332$.

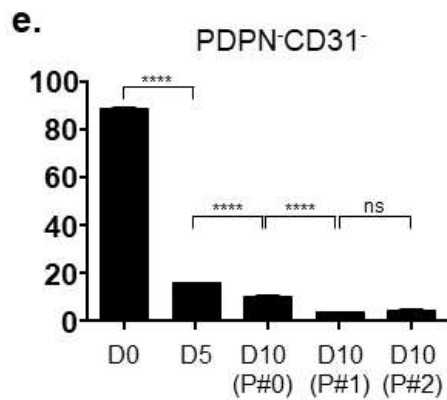
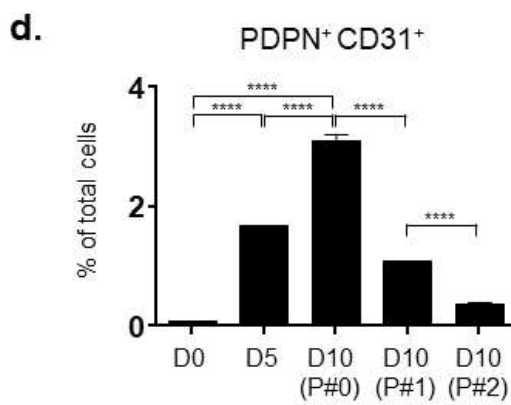
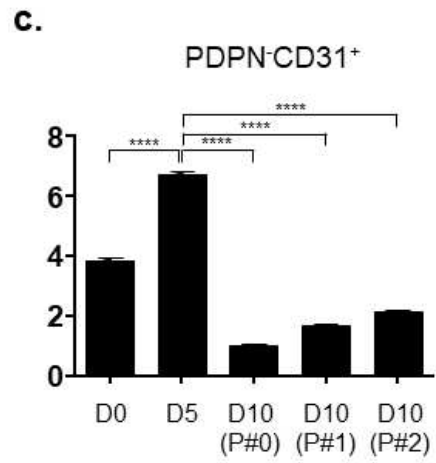
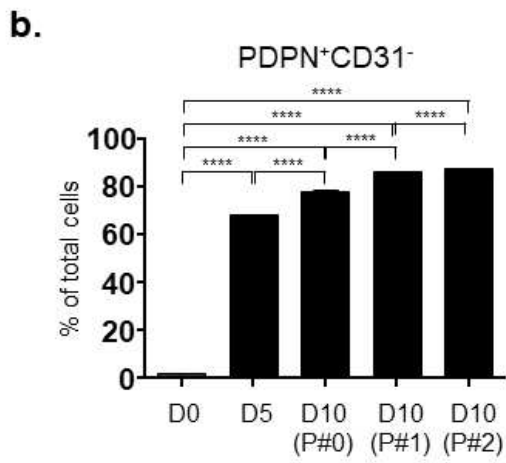
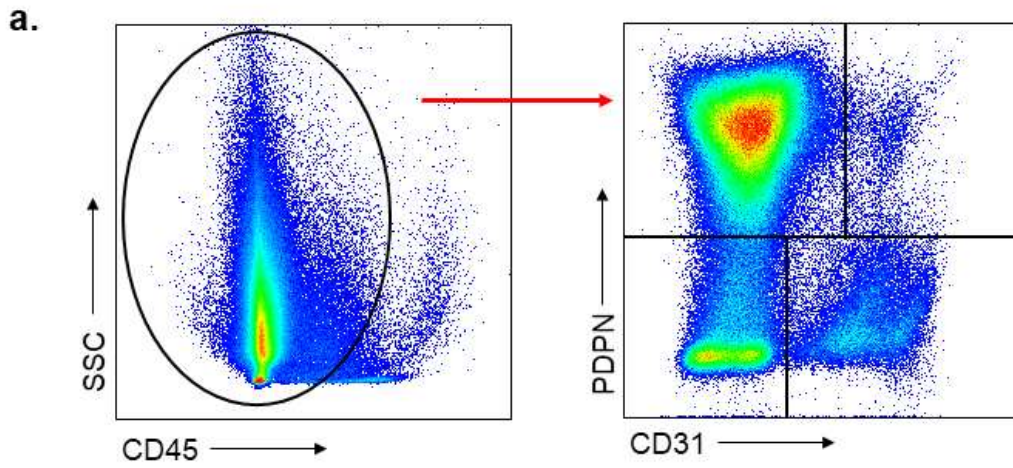


Figure 4. Characterization of CD45⁻ Non-Hematopoietic Cells in Cultured SVFs. a, Gating strategy for flow cytometry of CD45⁻ stromal cells: stromal subtypes were gated on CD45⁻, followed by analysis of PDPN and CD31. b, PDPN⁺CD31⁻ cells. c, PDPN⁻CD31⁺ cells, d, PDPN⁺CD31⁺ cells, e, PDPN⁻CD31⁻ double negative cells in the cultured SVFs on the indicated day and passage (n=3 per time points) **** $p < 0.0001$, *** $p < 0.0002$, ** $p < 0.0021$, * $p < 0.0332$.

PDPN+CD31- gated

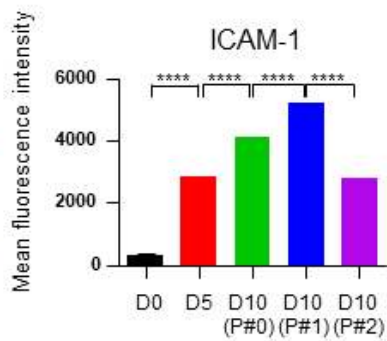
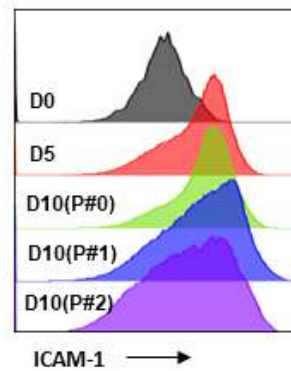
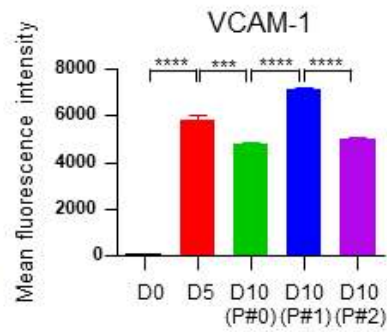
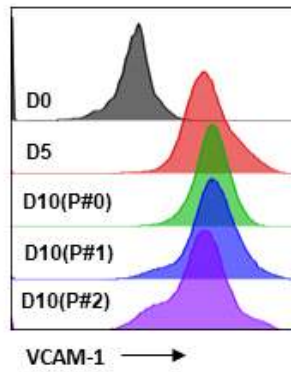
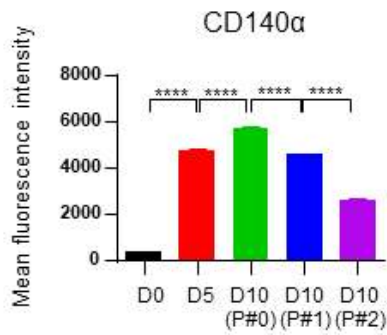
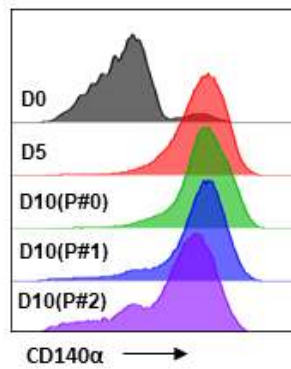
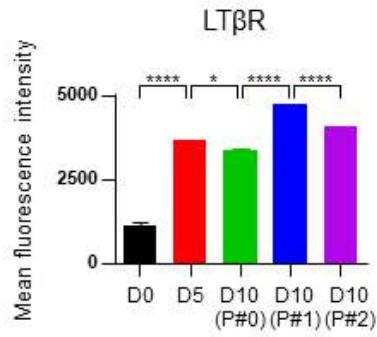
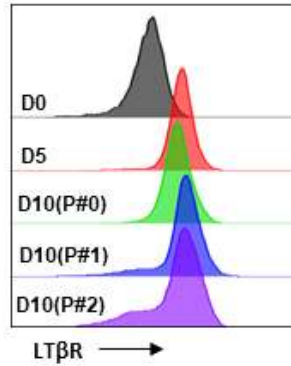
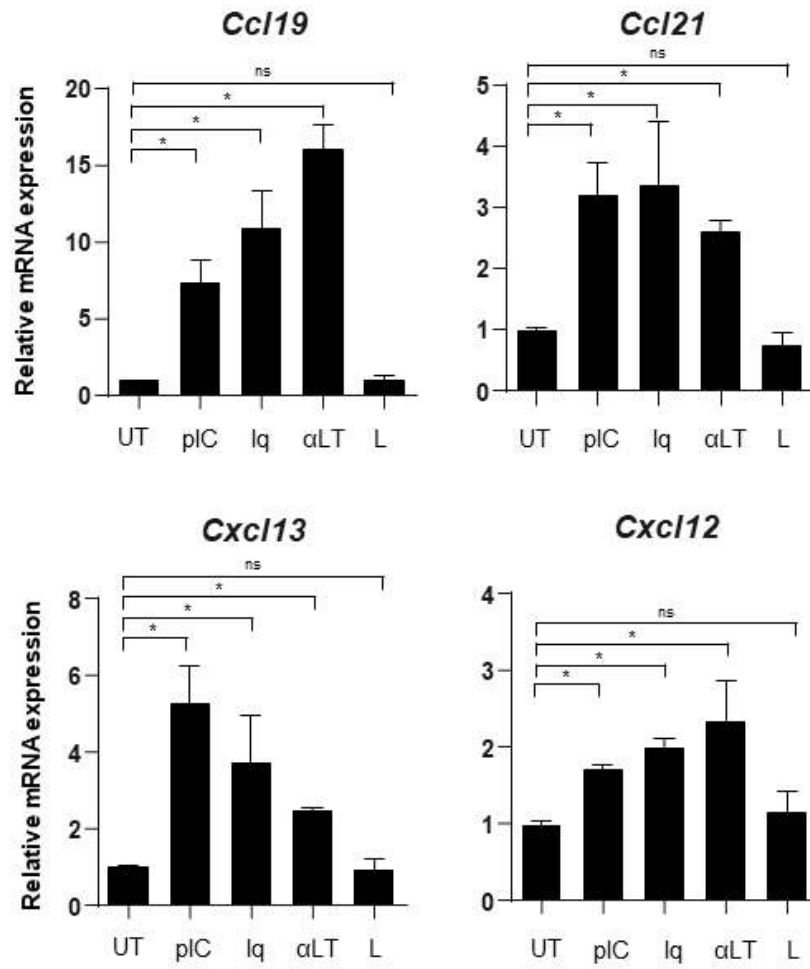
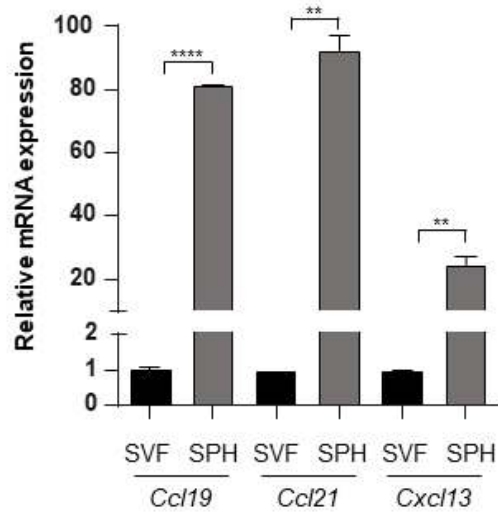


Figure 5. The Expression of LN FRC Markers Expressed on PDPN⁺ CD31⁻ Cells of the Cultured SVFs. Flow cytometry assessment was performed for lymphotoxin β receptor (LT β R) (Top panel), CD140 α (second panel), vascular cell adhesion molecule -1 (VCAM-1) (third panel), intracellular adhesion molecule -1 (ICAM-1) (last panel) in PDPN⁺ CD31⁻ gated cells. The histograms are representative plots of each markers (left). The bar graphs summarize the average of mean fluorescence intensity of each marker stained cells (right). **** $p < 0.0001$, *** $p < 0.0002$, * $p < 0.0332$ (ANOVA).

a.



b.



c.

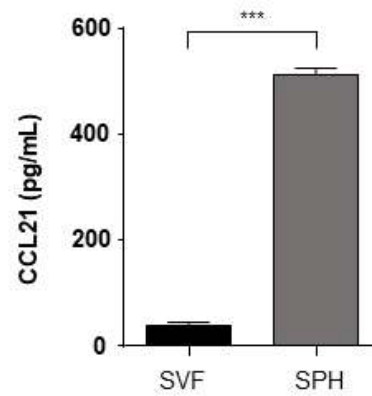


Figure 6. The Gene Expression of Chemokines in SVFs in Context-Dependent Manner. a, mRNA expression of the *ccl19*, *ccl21*, *cxcl13* and *cxcl12*, analyzed by qPCR (n=4), UT : untreated, pIC: polyI:C, Iq: imiquimod, α LT: anti-LT β R, L: LIGHT. * $p < 0.0332$ (Mann-Whitney test). b, Comparison of mRNA expression of *ccl19*, *ccl21* and *cxcl13* between 2D-cultured SVFs (SVF) and spheroid form of SVFs (SPH). **** $p < 0.0001$, ** $p < 0.0021$ (student' s *t*-test) c, Comparison of protein expression of CCL21 between SVF and SPH. *** $p < 0.0002$

2. SVF Spheroids Generate Vessels for Immune Cell Migration

Since SVFs express chemokines that might attract immune cells, the potential route of cell migration was investigated. SVFs are reported to be able to generate new blood vessels through the reassembly of blood endothelial cells.⁵⁵ The cultured SVFs also included endothelial cells (Fig. 4). To confirm whether the cultured SVFs form the vessel-like structure as a channel of immune cell migration, SVFs were incubated in collagen *in vitro*. Culturing single cells of the SVFs did not generate any structure that looked like a vessel, regardless of VEGF treatment (Fig. 7a). In contrast, when SVF SPHs were cultured in collagen, they formed the vessel-like structure which sprouted from the body on day 2 with VEGF and on day 3 without VEGF (Fig. 7b). Lymphatic vessel marker, LYVE-1 was detected at the tip of each bud. Moreover, the endothelial cell marker CD31 was dispersedly expressed throughout the body (Fig. 7c). There was a vacant core within the sprouts that were presumed to be the lumen in vessels (Fig. 8a). To confirm whether this vacant core indeed acts as a channel, the SVF SPHs were incubated in collagen for 3 days and were then given a fluid flow from top to bottom with particles 2 μm and 10 μm in size. The particles, mostly 2 μm beads, passed through the lumen of the vessel-like structures (Fig. 8b, c).

To further confirm the generation of vessels *in vivo*, SVF SPHs were transplanted into the kidney subcapsule of mice. The kidney subcapsular space was selected as an administration location because the kidney has a sufficient blood supply and its subcapsular space provides a shield for the transplant to nest, allowing for more accessible observation. Several vessels were

visible on the surface of the transplant after 2 weeks (Fig. 8d), and the generated vessels were positive for both VEGFR3 and CD31, markers of lymphatic and endothelial cells respectively (Fig. 8e). Moreover, CD3⁺ T cells seemed to interact with CD31⁺ cells for migration in the frozen section image (Fig. 8f). The analysis of mRNA expression between 2D-cultured SVFs and SVF SPHs revealed that 11 genes related to angiogenesis were up-regulated in SVF SPHs and 5 genes were down-regulated in SVF SPHs, compared to SVFs grown in monolayer (Fig. 9a, b). Besides, the percent of CD31⁺ endothelial cells in SVF SPHs slightly increased compared to SVFs in flow cytometry analysis (Fig. 9c). Collectively, the cultured SVFs were capable of vessel generation that would potentially work as a channel for immune cell migration. Moreover, 3D spheroid form of SVFs showed enhanced transcriptional and translational expressions of angiogenesis and lymphangiogenesis to 2D cultured SVFs.

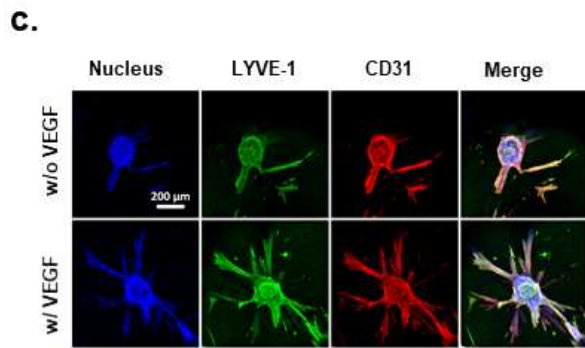
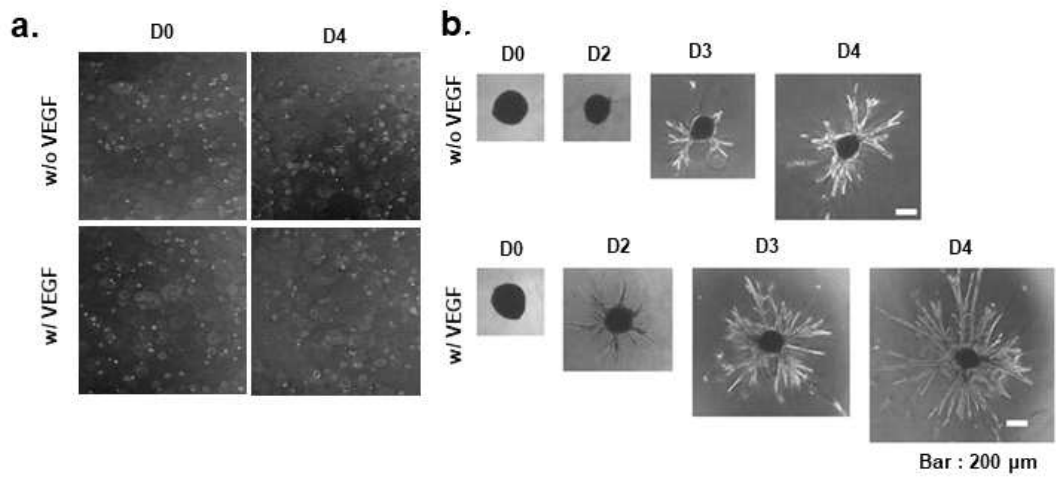


Figure 7. The Spheroid Form of SVFs Can Generate Vessel-Like Structures. The single cells (a) and spheroids (b) of SVFs were incubated in 3 mg/mL collagen type I with or without 100 ng/mL of VEGF-A and -C contained medium for 4 days. Scale bar: 200 μ m. c, Immunofluorescence staining of vascularized SVF spheroids in b. Scale bar: 200 μ m.

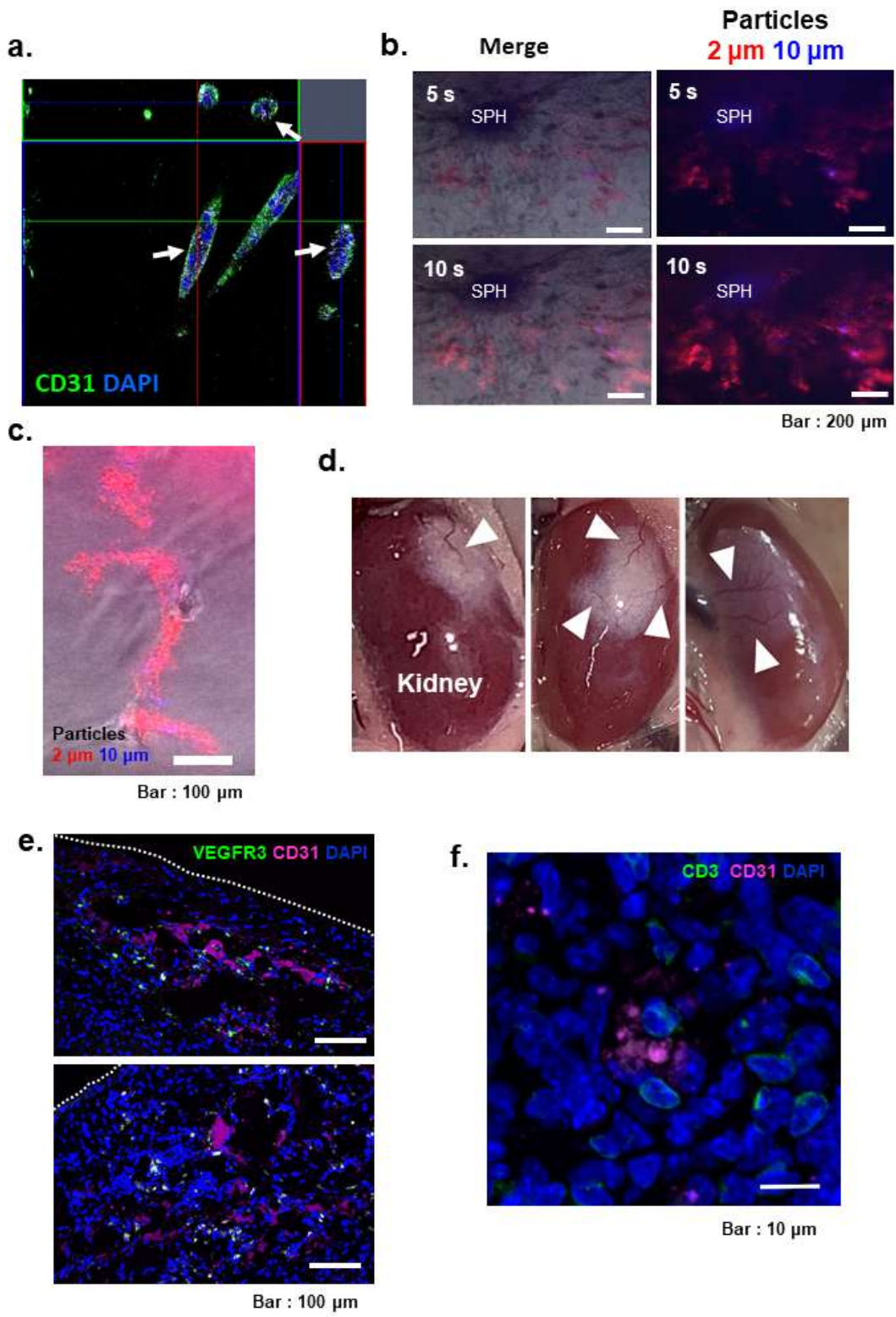


Figure 8. The Vessel-Like Structures Formed from SVF Spheroids Could Act as Migration Routes of Immune Cells. a, Immunofluorescence staining of a vascularized SVF spheroid (SPH) section in 7b. The arrows indicate the lumen of sprout inside. b, Fluorescence microscopy images of 3D-cell migration assay in microfluidic platform. The pictures were taken at 5 s (upper panel) and 10 s (lower panel). Scale bar: 200 μm . c, The magnified picture of the result in b. Scale bar: 100 μm . d, *In vivo* vessel generation the transplantation of SVF SPHs into kidney subcapsular space. The arrowheads indicate the blood vessels on the surface of the transplants in kidney subcapsules. e, Confocal images of the sections of the transplants in d. The dotted lines (white) indicate the boundary of transplants. Scale bar: 100 μm . f, Confocal image of the transplant in d which shows the interaction between CD31⁺ endothelial cells and CD3⁺ T cells. Scale bar: 10 μm .

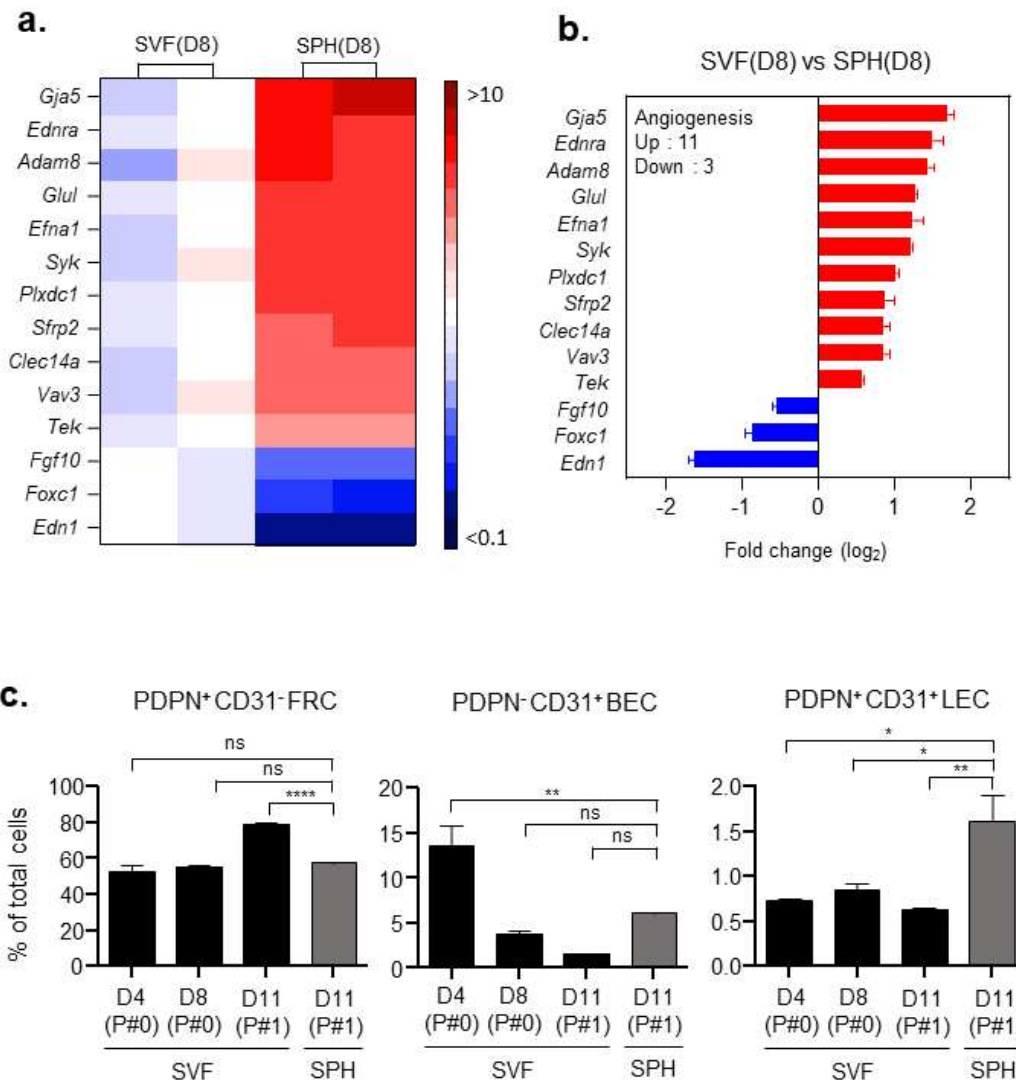


Figure 9. Comparison of SVFs and Spheroid Form of SVFs. a, Heatmaps depicting log₂ expression fold changes of differentially expressed genes related to angiogenesis in SVFs and SVF spheroids (SPH). ($p < 0.05$, $n = 2$) b, Summary of the result in a. ($p < 0.05$, $n = 2$) c, Quantification of stromal-like subtypes in cultured SVFs at indicated time points and subculture passages (passage 0 (P#0), passage 1 (P#1)) . **** $p < 0.0001$, ** $p < 0.0021$, * $p < 0.0332$.

3. SVF Spheroids Attract Dendritic Cells and Enhance DC–T Cell Interactions

mRNA transcriptome analysis revealed that the SVF SPHs showed a significant increase in the expression of several secreted factors that are essential for cell migration when compared to those of the isolated SVFs on day 0 (Fig. 10a). This increase in expression correlated with the expansion of stromal-like cells in cultured SVFs (Fig. 1–2). Genes related to secreted factors such as chemokines, cytokines, growth factors, and extracellular matrix proteins were categorized based on p -value < 0.05 . The gene expression of vascular endothelial growth factor α (*Vegfa*) and platelet-derived growth factor C (*Pdgfc*), which are crucial for angiogenesis, were up-regulated in SVF SPHs, consistent with previous results (Fig. 7, 8). The expression of matrix metalloproteinase 8, 10, and 13 also significantly increased in SVF SPHs, indicating that matrix metalloproteinases could degrade the extracellular matrix and potentially allow cells to penetrate their way to migrate.^{56,57} Furthermore, genes related to the recruitment and activation of immune cells (*Spp1*, *Ccl8*, *Cxcl5*, *Postn*, *Cxcl16*, *Ccl17*) were upregulated in the spheroid form of SVFs. In particular, *Spp1*, also known as osteopontin, was the most up-regulated gene in SVF SPHs compared to SVFs on day 0. Osteopontin is known to regulate the maturation and survival of dendritic cells.⁵⁸ To examine the translational expression of osteopontin, its concentrations in the culture supernatants were measured. The amount of osteopontin was the highest in SVF SPHs, consistent with the transcriptome analysis (Fig. 10b). Taken together, RNA transcriptome analysis of SVF spheroids revealed that SVFs

were capable of expressing a variety of secretion molecules required for the activation and recruitment of immune cells.

To examine whether SVF SPHs can truly recruit immune cells according to their transcriptome analysis, a chemotaxis assay was conducted for 24 h. Indeed, SVF SPHs attracted the splenocytes in the counterpart across the collagen layer (Fig. 11a). To determine which immune cells were preferentially attracted to SVF SPHs, CD3⁺ T cells, and bone marrow-derived dendritic cells (BMDCs) were sorted and analyzed by chemotaxis assay. Since SVF SPHs secreted CCL21 and osteopontin (Fig. 6c, 10b), T cell and BMDC migration were anticipated. Intriguingly, however, only BMDCs showed significant migration ability towards SVF SPHs, not T cells (Fig. 11b–d).

To confirm the ability of SVF to recruit immune cells *in vivo*, the spheroids of SVF were transplanted into the kidney subcapsule in the mice. Consistent with the *in vitro* results of migration assay, the transplantation of SVF SPHs alone rarely recruited CD3⁺ T cells (Fig. 12a). Interestingly, a lot of CD3⁺ T cells were recruited in the group of SVF SPHs transplanted with mature BMDC (mDC) (Fig. 12c). CD3⁺ T cells were observed at the boundary between the kidney tissue and the transplant, as well as throughout the entire field of the transplant. T cells were intermingled with PDPN⁺ SVF cells (Fig. 12c). Although CD3⁺ T cells were also observed in the group of mDC alone (Fig. 12b), the number and area of migrated T cells were significantly less than those of the SVF SPHs with mDC group (Fig. 12b–d). The transplant included CD4⁺, CD8⁺ T cells, and CD11c⁺ dendritic cells (Fig. 13a, b). For a quantitative examination of cells in the transplant, the distribution of cells

was analyzed by flow cytometry. As expected, the group of SVF SPHs with mDC contained mostly CD3⁺ T cells (Fig. 13d), even though the CD45⁺ hematopoietic population in the group of SVF SPHs with mDC was not significantly higher than the group of mDC alone (Fig. 13c). B220⁺ B cells were scarcely observed in all of the groups (under 0.2% of total cells) (Fig. 13e). Moreover, CD4⁺ T cells were the most recruited in the group of SVF SPHs with mDC (Fig. 13f). On the other hand, the frequency of CD8⁺ T cells in the group of SVF SPHs with mDC was not significantly higher than that in the group of mDC alone (Fig. 13g). In terms of the myeloid population, about 2% of CD11c⁺ dendritic cells of the total cells were recruited in the group of SVF SPHs with mDC (Fig. 13h), consistent with that SVF SPHs recruited BMDCs *in vitro* (Fig. 11c, d). Approximately 1% of F4/80⁺ macrophages were detected in all of the groups (Fig. 13i). CD11b⁺ Gr-1⁺ neutrophils were only significantly recruited in mDC transplant group (Fig. 13j). Therefore, SVFs attract DCs, potentially by expression of various chemokines. mDCs are the ones which attract T cells. Yet the presence of SVFs with DCs significantly enhanced CD3⁺ T cell infiltration. These might indicate that SVFs sustain T cells recruited by DCs longer, providing a niche for DCs to interact with infiltrated T cells.

The infiltrated T cells were more deeply analyzed using effector and memory T cell markers (i.e. CD62L⁻CD44⁺ effector cells, CD62L⁺CD44⁺ memory cells, CD62L⁺CD44⁻ naive cells). The frequency of the effector T cells tended to be the highest among the recruited T cells (Fig. 14). The percentage of CD4⁺ effector, memory, and naive T cells in the group of SVF SPHs

with mDC were significantly higher than those in other groups (Fig. 14a). In the case of CD8⁺ effector and memory T cells, despite not being significantly higher, showed a similar trend to CD4⁺ T cells where the highest frequency was observed in the group of SVF SPHs with mDC (Fig. 14b).

Collectively, this data (Fig. 10–14) implied that SVFs attract DCs and assist DC–T cell interaction, acting as a hub like LNs. Therefore, T cells get better chances to interact with DCs, and are readily differentiated into CD44⁺ effector T cells and potentially launch an improved immune response.

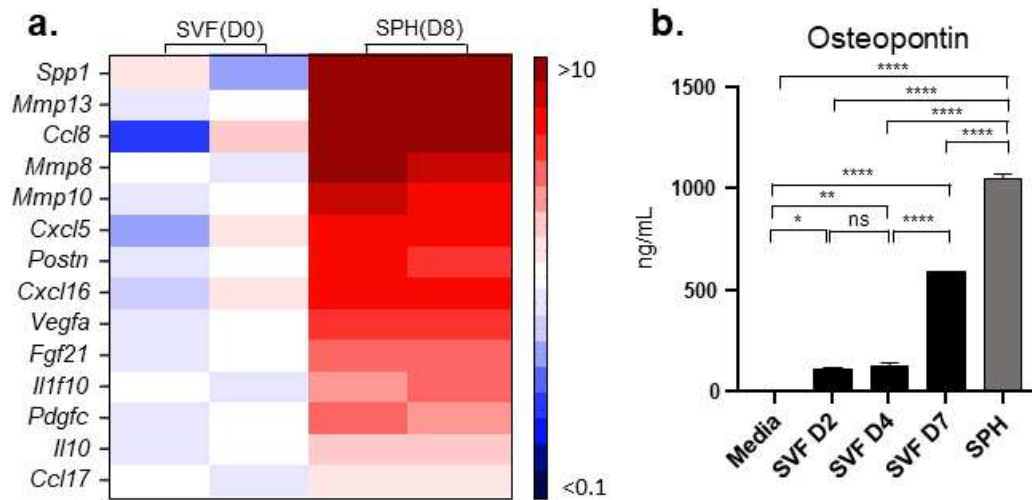


Figure 10. Gene Expression Analysis of SVF Spheroids. a, Heatmaps depicting differentially expressed genes related to secretion factors in the cultured SVFs. The data was compared between the gene expression of SVFs on day 0 and SVF spheroid (SPH) on day 8 after isolation ($p < 0.05$, $n = 2$). b, ELISA quantification of Osteopontin. **** $p < 0.0001$, ** $p < 0.0021$, * $p < 0.0332$.

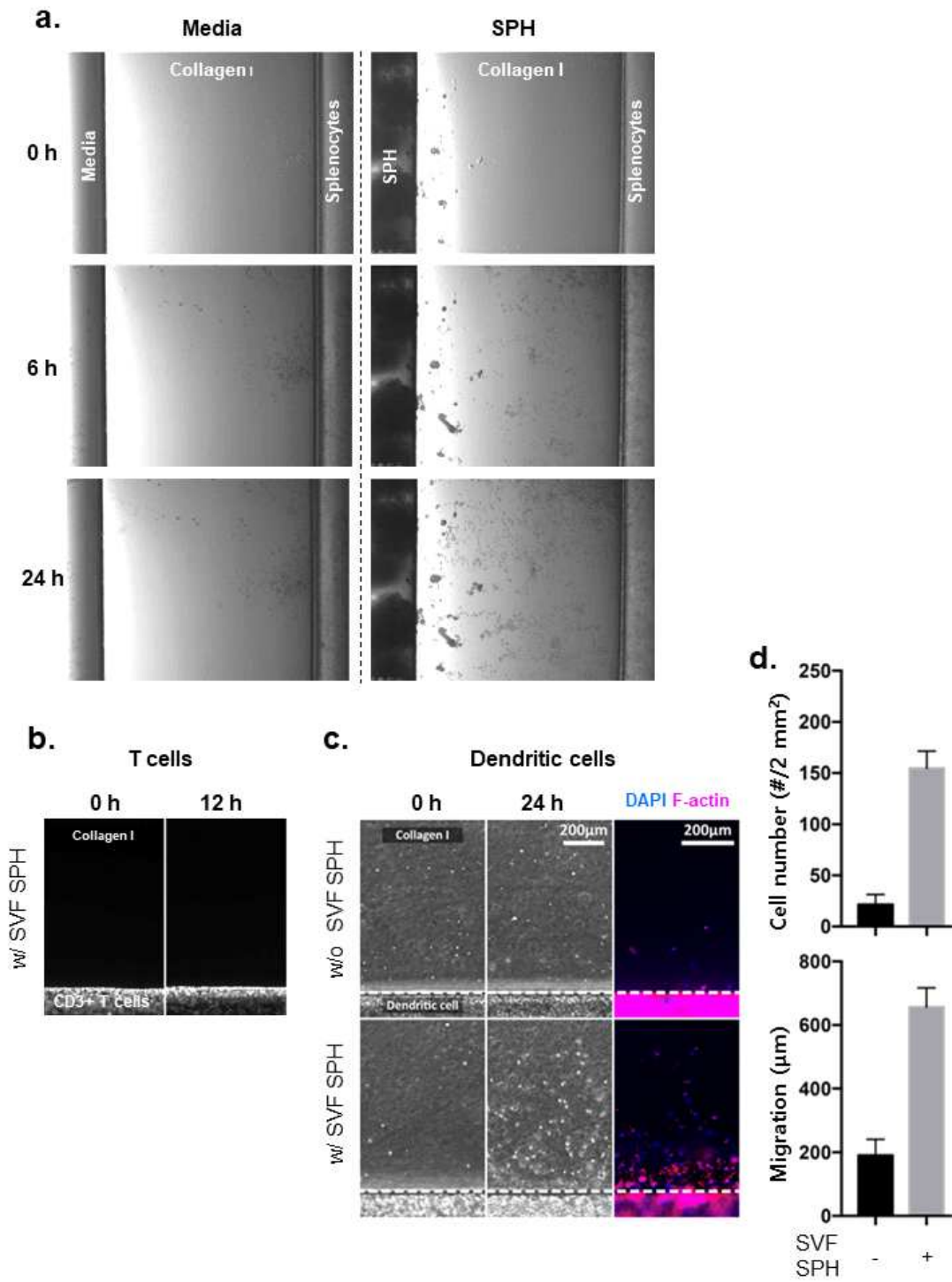


Figure 11. SVF Spheroids Can Recruit Dendritic Cells. a, Confocal images of chemotaxis assay of splenocytes induced by SVF spheroids (SPH). SPH and splenocytes were placed in the left and right of the chemotaxis kit with 1.5 mg/mL of Type I Collagen solution filled in between two. The migration of splenocytes was observed for 24 h. b and c, Confocal images of chemotaxis assay of T cells and dendritic cells induced by SPH. d. Quantification of migrated dendritic cells.

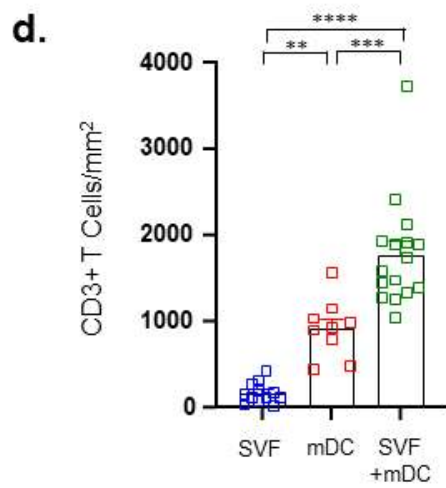
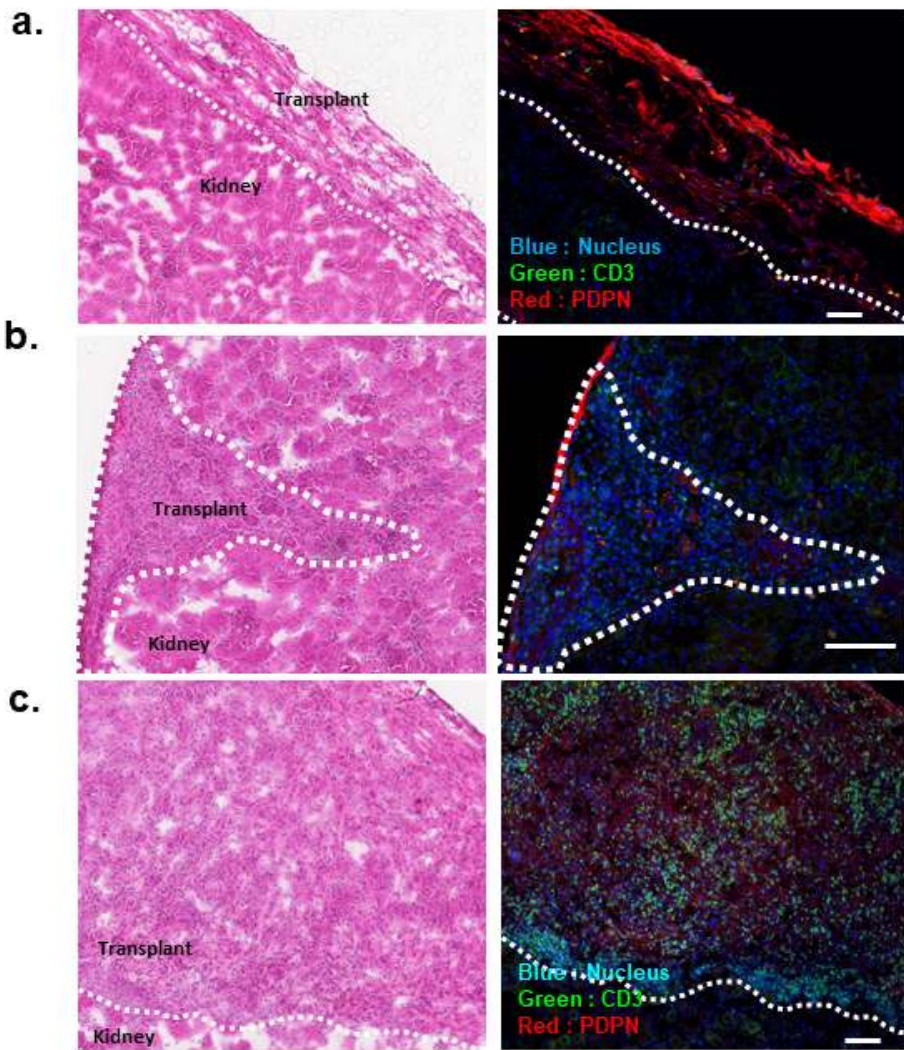


Figure 12. *In vivo* Organogenesis by Transplantation of SVF Spheroids and Dendritic Cells into the Kidney Subcapsular Space. a–c, Sectioned images of the grafts of SVF SPH or DCs in the kidney subcapsule after 2 weeks. Haemotoxylin and Eosin staining (left column) and confocal images (right column) of a, SPH transplanted group, b, DC transplanted group, c, SPH and DC transplanted group (n=3 in each group). The white dash lines depict the outline of each graft in the sections. d, Quantification of CD3⁺ T cells in field of view per area (mm²) in each image in a–c. The images were analyzed by IMARIS ver 9.3 (n=12 in SPH transplanted group (SVF), n=9 in DC transplanted group (mDC), n=16 in SPH with mDCs–transplanted group (SVF+mDC) *****p*<0.0001, ****p*<0.0002, ***p*<0.0021.

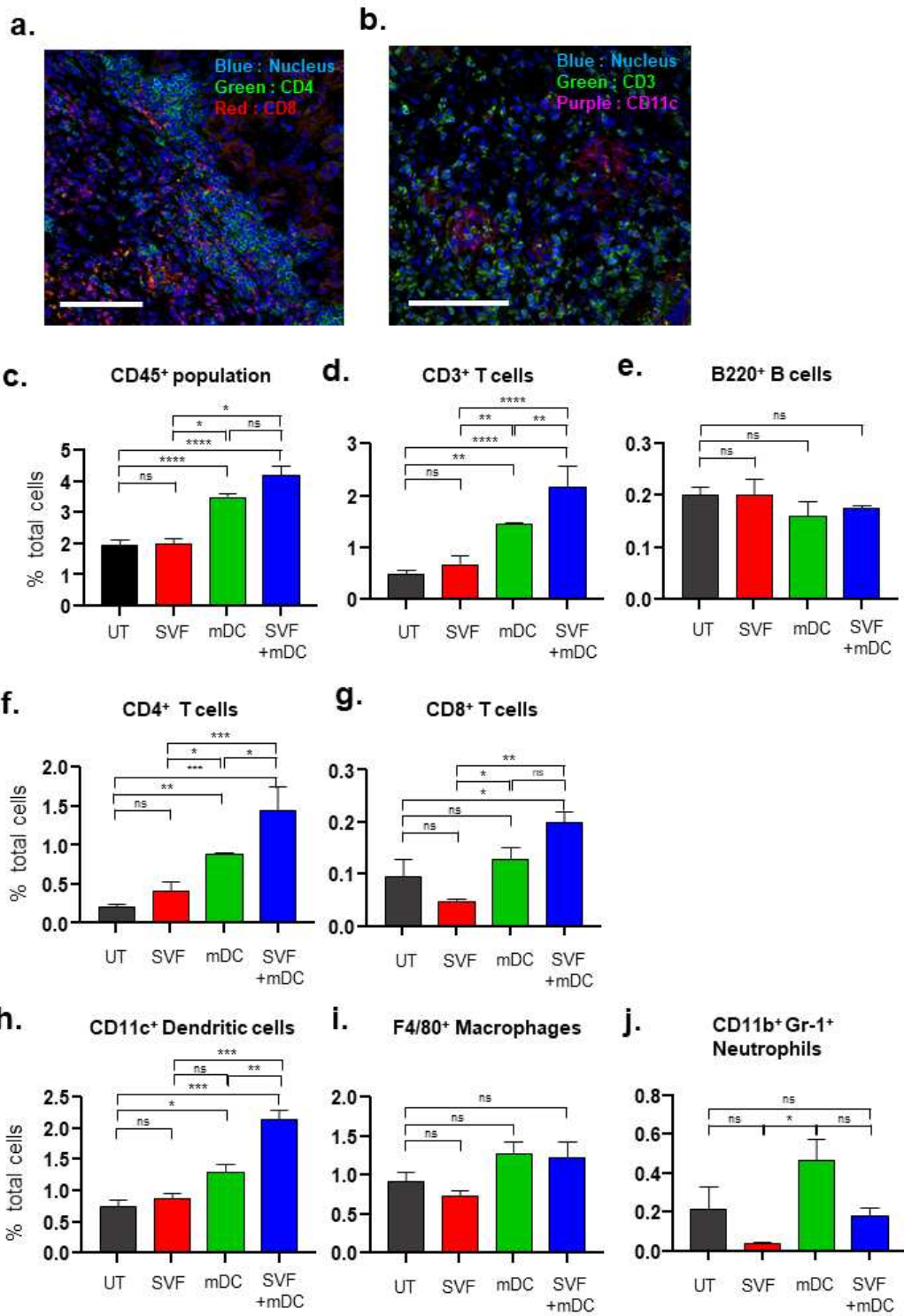


Figure 13. Analysis of Cell Population of the Transplants. a and b, Representative confocal images of SPH with DC-transplanted group (SVF+mDC). a, CD4⁺ (green) and CD8⁺ (red) T cells were stained. Scale bar: 100 μ m. b, CD3⁺ (green) T cells and CD11c⁺ (purple) DCs were stained. Scale bar: 100 μ m. c-j. Quantitative cell composition analysis of transplants by flow cytometry. c, CD45⁺ population of transplants. d, CD3⁺ T cells. e, B220⁺ B cells. f, CD4⁺ T cells. g, CD8⁺ T cells. h, CD11c⁺ dendritic cells. i, F4/80⁺ macrophages. j, CD11b⁺Gr-1⁺ Neutrophils. UT: untreated group (n=3), SVF: SVF SPH alone-transplanted group (n=3), mDC: mature DC alone-transplanted group (n=3), SVF+mDC: SVF SPH with mDCs-transplanted group (n=2). **** p <0.0001, *** p <0.0002, ** p <0.0021, * p <0.0332.

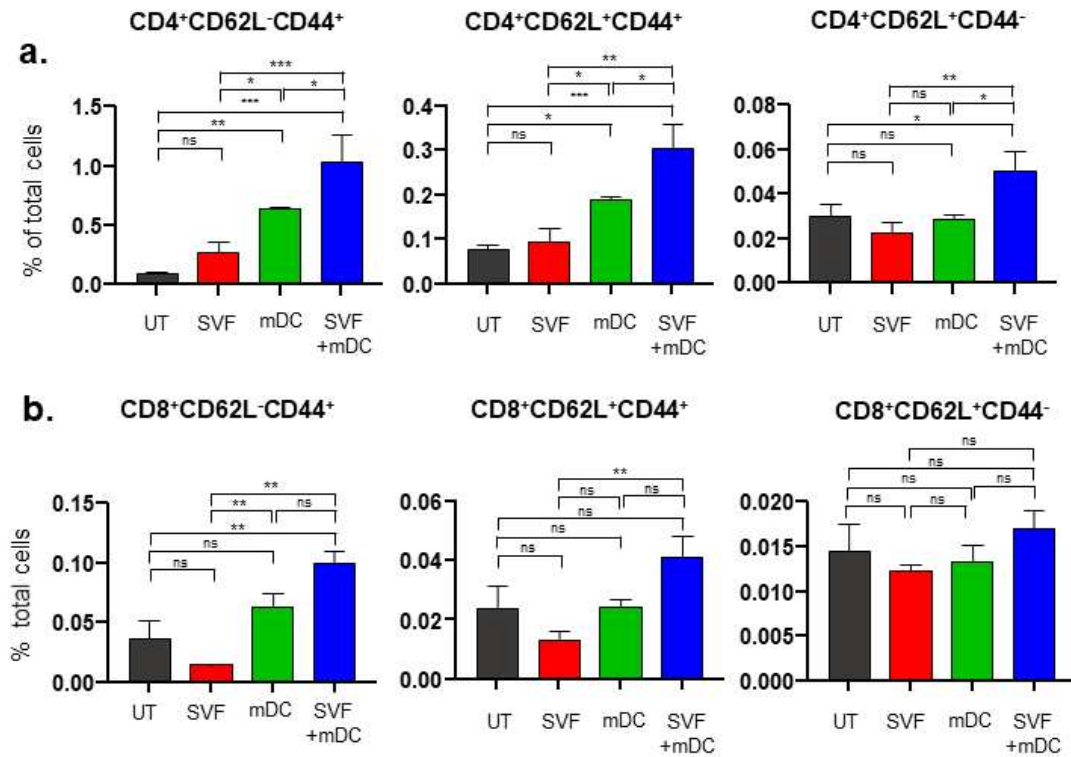


Figure 14. Phenotypes of Infiltrated T Cells in Transplants. a and b. The proportion of the effector T cells (CD62L⁻CD44⁺), memory T cells (CD62L⁺CD44⁺) and naive T cells (CD62L⁺CD44⁻) in CD4⁺ T cells (a) and CD8⁺ T cells (b). **** $p < 0.0001$, *** $p < 0.0002$, ** $p < 0.0021$, * $p < 0.0332$.

4. Enhancement of Antigen-Specific T Cell Responses by SVF Spheroids and DC Complex

To elucidate the mechanism of how SVFs regulate DC-T cell interaction, SVFs and DCs were co-cultured, and mRNA expression was analyzed by RNA sequencing (Fig. 15). The level of various chemokines was upregulated in SVFs co-cultured with DCs, but especially the expression of *ccl20*, *ccl22*, *cxcl10*, and *cxcl16* which attract T cells⁵⁹ increased, consistent with T cell recruitment *in vivo* (Fig. 12c). Moreover, immunostimulatory factors (i.e. *il6*, *il12b*, *tnf*, *cd40*, and *icosl*) and the T cell survival factor (i.e. *il7*) were upregulated in SVFs co-cultured with DCs, compared to that of SVFs alone. An immunosuppressive factor, *nos2* was also upregulated in SVFs incubated with DCs, consistent with the immunosuppressive ability of FRCs on activated T cells.⁶⁰ Additionally, the expression of cytokines related to vascularization such as *vegfa*, *vegfc*, and *pdgfb*^{61, 62} was elevated. The gene expression of adhesion molecules (i.e. *icam1*, *pdpn*, *pecam1*, *vcam1*) also increased (Fig. 15a). Based on this transcriptomic analysis, it is suggested that SVFs incubated with DCs can recruit T cells via the elevated expression of chemokines and can retain the cells on-site by expressing the adhesion molecules, as well as support the immune response and survival for T cells.

Next, the transcriptome of DCs co-cultured with SVFs showed that the expression of T cell-attractant chemokines (i.e. *ccl3*, *ccl4*, *ccl17*, *ccl20*, *cxcl12*)⁵⁹ and immunostimulatory factors (i.e. *il1a*, *il1b*, *il6*, *il12a*, *cd80*) was elevated in DCs with SVF compared to that of DCs alone. Therefore, DCs incubated with

SVFs can recruit T cells via chemokines and activate T cell response by expressing inflammatory cytokines and a co-stimulatory factor (Fig. 15b).

Furthermore, the magnitude of activation of DCs cultured with SVFs for 24 h was analyzed by flow cytometric analysis. The level of CD40, CD80, MHCII, and DC-SIGN was significantly enhanced in mDCs incubated with SVFs compared to that of mDC alone (Fig. 16a). The expression of CD80 was consistent with transcriptomic analysis (Fig. 15b). Since the SVFs sustained the infiltrated T cells in the graft for 2 weeks (Fig. 12c, d), the SVFs improved survival of immune cells was tested. DCs and splenocytes were co-cultured with SVFs for 1 day and 7 days, respectively. The survival rate of DCs and splenocyte was measured by 7-AAD staining. The death rate of DCs co-cultured with SVFs (7-AAD⁺ DCs) was only half of that of immature DCs or mature DCs (Fig. 16b). The survival rate of splenocytes co-cultured with SVFs for 7 days (35%) was approximately 7 times higher than that of splenocytes cultured alone (5%) (Fig. 16c). These results showed that mature DCs co-cultured with SVFs are in a more activated state with a longer life span. Therefore, these DCs would be more capable of effective T cell priming, resulting in an improvement of the antigen-specific T cell response.

Hence, the next question, whether or not the SVF SPHs with mDC could enhance antigen-specific T cell response, was asked. To load antigens to DCs, Fe₃O₄-ZnO core-shell nanoparticles (FZ-NPs) with a uniform size of 10.5±1.5 nm were used (Fig. 17a-c). As shown in the energy dispersive X-ray spectroscopy (EDS) mapping images in Fig. 17d-f, the boundary between ZnO

and Fe_3O_4 is clearly distinguished and ZnO covers the entire surface of the Fe_3O_4 core. The thickness of ZnO is about 10% of the core size, forming a 1.9 nm-layer. Indicated combinations in Fig. 16 (untreated group, SVF SPHs with ovalbumin (OVA), mDCs pulsed with OVA, and SVF SPHs and mDC pulsed with OVA) were transplanted into the kidney subcapsule once every other week for 4 weeks (Fig. 18a). 1×10^6 DCs were pulsed with 20 μg ZBPOVA bound to 100 μg FZ-NPs. The portion of OVA-specific CD4^+ and CD8^+ T cells in the group of mDCs with SVF SPHs was significantly higher than that of other groups, measured by OVA peptide-loaded MHC tetramer staining (Fig. 18b). Therefore, SVFs enhance DC-T cell interaction by augmenting the activation and life span of DCs, significantly advancing the antigen-specific T cell response.

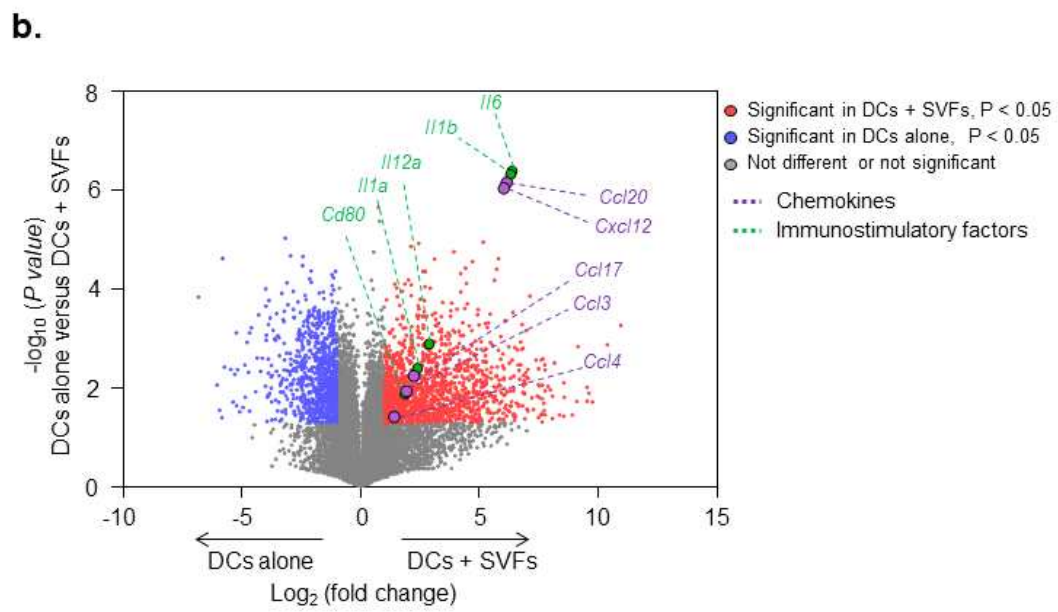
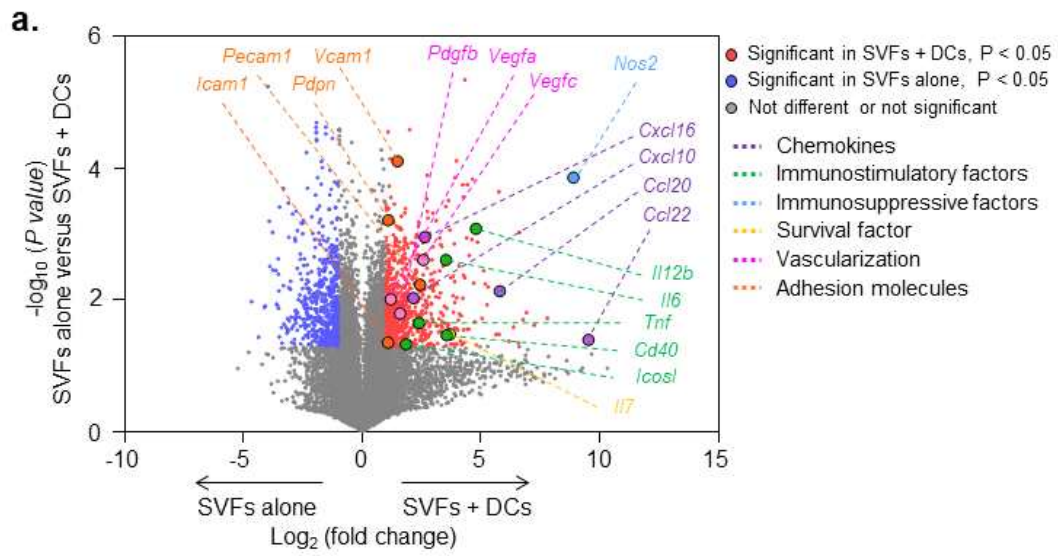


Figure 15. The Transcriptomic Analysis of Co-Cultured SVFs and DCs. a, The volcano plot of transcriptome displaying upregulated genes in SVFs alone-cultured for 24 h (blue, p -value < 0.05 and $\log_2 > 1$) or SVFs co-cultured for 24 h with mature DC (mDC) (red, p -value < 0.05 and $\log_2 > 1$) (n=2 in each group). The gene sets are marked at the right side. b. The volcano plot of transcriptomic data that show upregulated genes in mDCs alone-cultured for 24 h (blue, p -value < 0.05 and $\log_2 > 1$) or mDCc co-cultured for 24 h with SVFs (red, p -value < 0.05 and $\log_2 > 1$) (n=2 in each group).

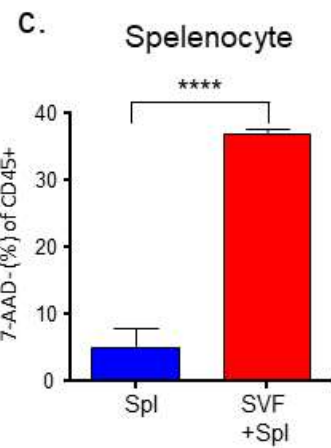
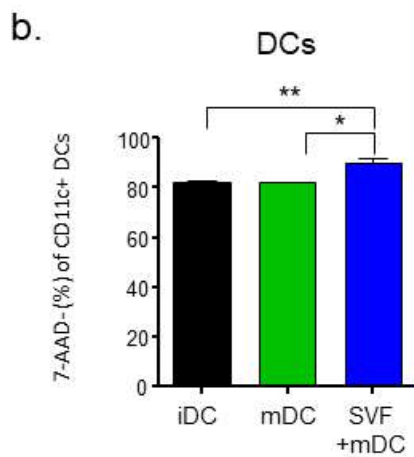
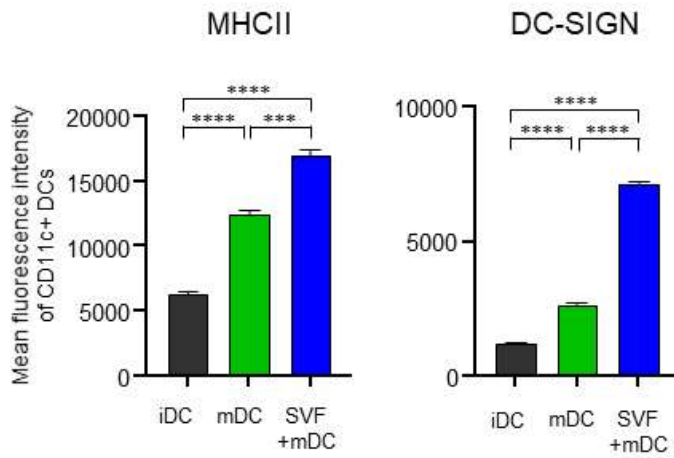
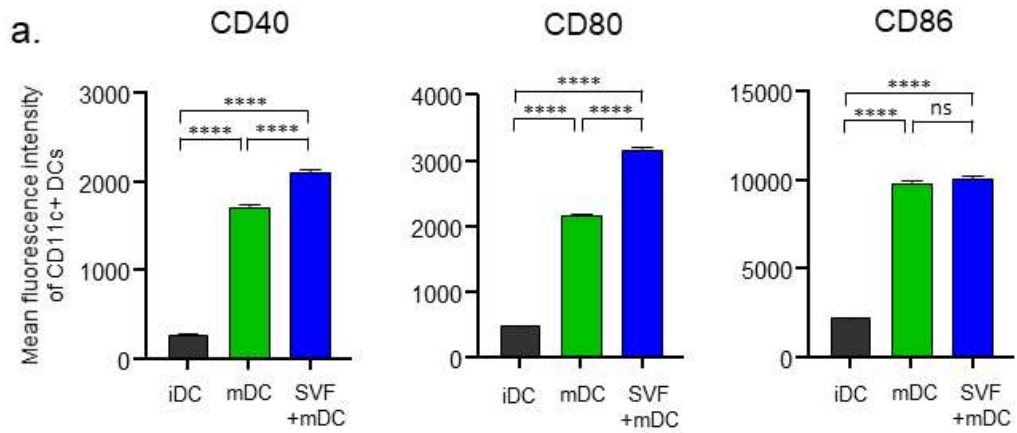


Figure 16. SVFs Regulate Activation and Survival of Immune Cells. a, Flow cytometry measurements of dendritic cell activation markers (CD40, CD80, CD86, MHCII and DC-SIGN) of CD11c⁺ DCs co-cultured with SVFs for 24 h. iDC: immature DC alone-cultured group (n=3), mDC: mature DC alone-cultured group (n=3), SVF+mDC: mDC co-cultured with SVF group (n=3). **** $p < 0.0001$, *** $p < 0.0002$. b and c, Survival of DCs and splenocytes cultured with and without SVFs. b, DCs were incubated alone or with SVFs for 24 h. c, Splenocytes were incubated alone or with SVFs for 7 days. **** $p < 0.0001$, ** $p < 0.0021$, * $p < 0.0332$ by ANOVA.

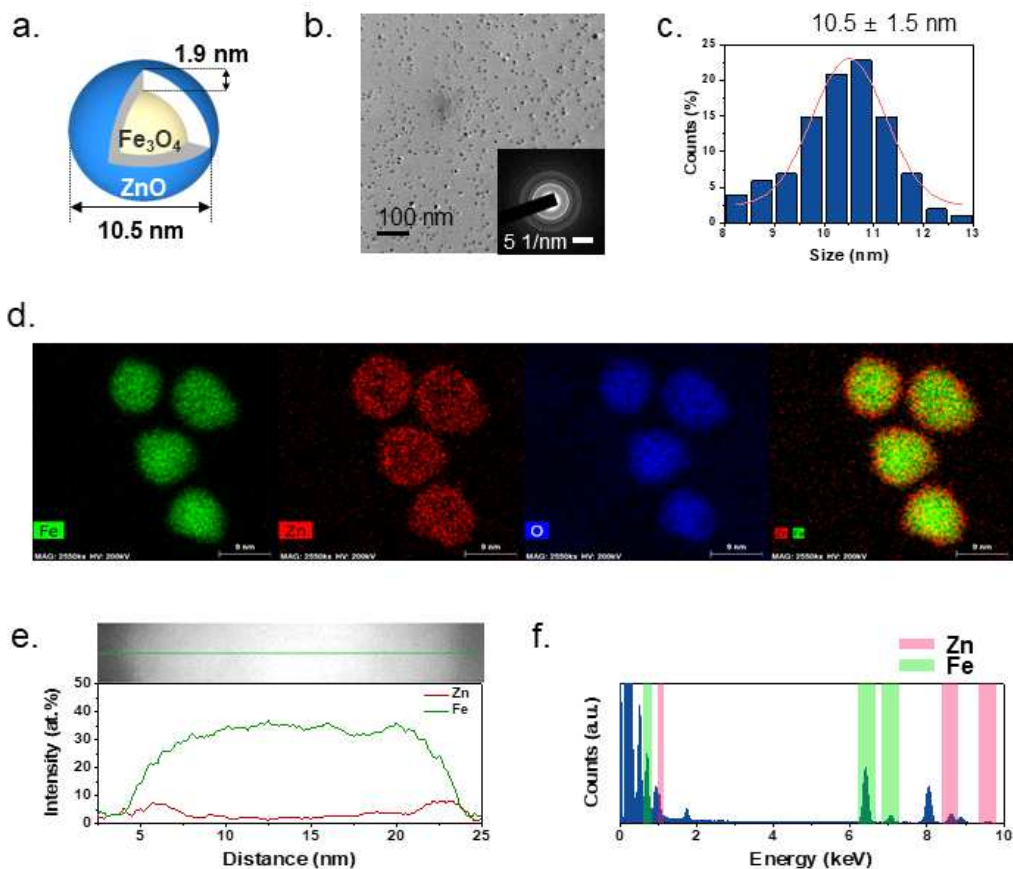
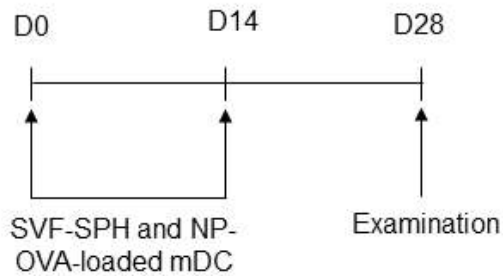


Figure 17. Characteristics of $\text{Fe}_3\text{O}_4\text{-ZnO}$ Core-Shell Nanoparticle. a, Diagram of the $\text{Fe}_3\text{O}_4\text{-ZnO}$ core-shell nanoparticle. b, TEM image and SAED pattern of $\text{Fe}_3\text{O}_4\text{-ZnO}$ core-shell nanoparticle. c, Size distribution of $\text{Fe}_3\text{O}_4\text{-ZnO}$ core-shell nanoparticle. The mean value of diameter was obtained by fitting the counts using gaussian function. d, Elemental mapping images of $\text{Fe}_3\text{O}_4\text{-ZnO}$ core-shell nanoparticle; Fe (green), Zn (red), Oxygen (blue). e, Energy Dispersive Spectrometry (EDS) line scan of the elemental composition; Fe (green), Zn (red). f, Point-probe analysis of EDS that collected the signal from a single nanoparticle.

a.



b.

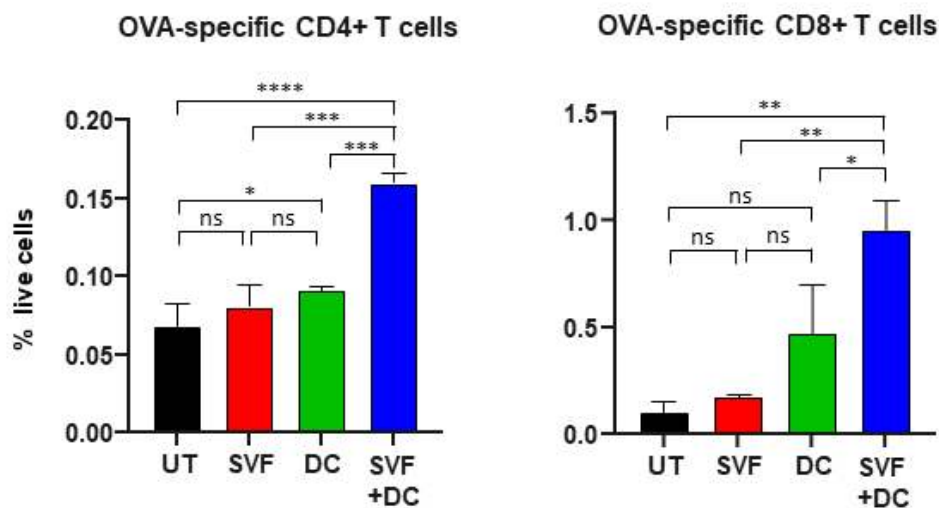
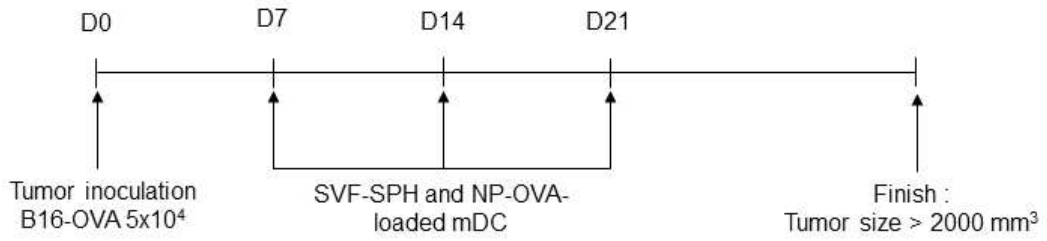


Figure 18. The Administration of SPH with DCs Enhances the Antigen-Specific Immune Response *in vivo*. a, Schedule of immunization. The combination of SPH and ZBPOVA (OVA)-pulsed DCs was immunized twice with two-week intervals through renal subcapsular transplantation in mice. b, Quantification of live OVA-specific CD4⁺ and CD8⁺ T cells. UT: untreated group (n=3), SVF: SVF SPH alone-transplanted group (n=3), mDC: mature DC alone-transplanted group (n=3), SVF+mDC: SVF SPH with mDCs-transplanted group (n=3), *****p*<0.0001, ****p*<0.0002, ***p*<0.0021, **p*<0.0332 by one-way ANOVA.

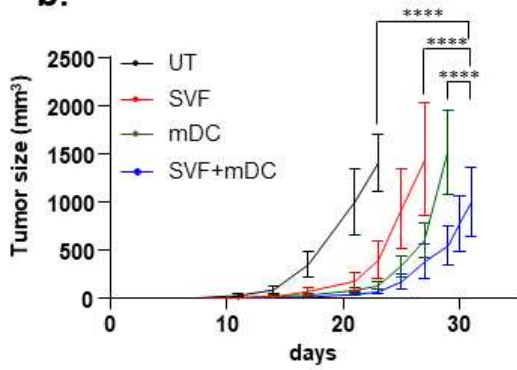
5. Anti-Tumor Effect of SVF Spheroids and DC Complex

Given that SVFs could implement an enhanced T cell response by efficiently priming DCs, DC-based cancer immunotherapy including SVFs was designed. To investigate the anti-tumor effect of SVF SPHs with dendritic cells, SVF SPHs with OVA-loaded dendritic cells were transplanted into the kidney subcapsular space once a week for 3 weeks (at day 7, 14, 21) after 7 days of OVA-expressing B16 melanoma inoculation (day 0) (Fig. 19a). The tumor growth increased the fastest in the untreated group, followed by the group with SVF SPHs and NP-OVA, with NP-OVA-loaded mature dendritic cells, and with SVF SPHs and OVA-loaded dendritic cells in order (Fig. 19b, c). Moreover, all of the mice that were treated with SVF SPHs and mDCs survived until 32 days after tumor inoculation. On the other hand, a 0%, 20%, and 40% survival rate were observed in the untreated group, the group with SVF SPHs and NP-OVA, and the group with OVA-loaded dendritic cells, respectively (Fig. 19d). These results showed that DCs transplanted with SVF SPHs strongly induced an anti-tumoral immune response and that SVFs significantly improved DC-based immunotherapy.

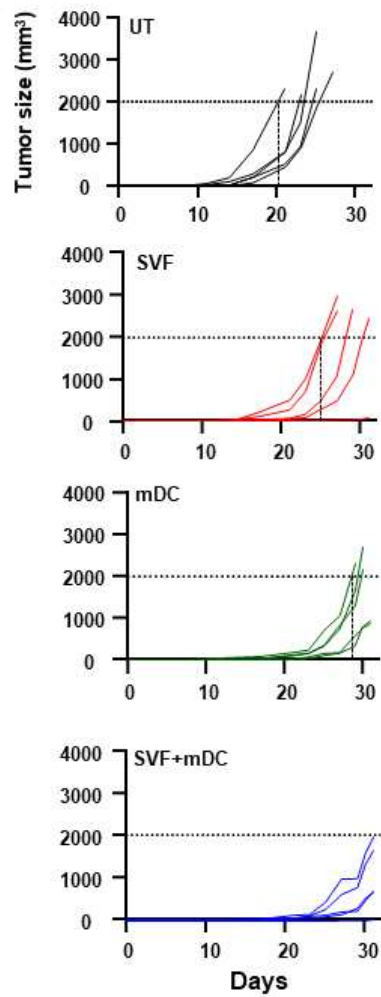
a.



b.



c.



d.

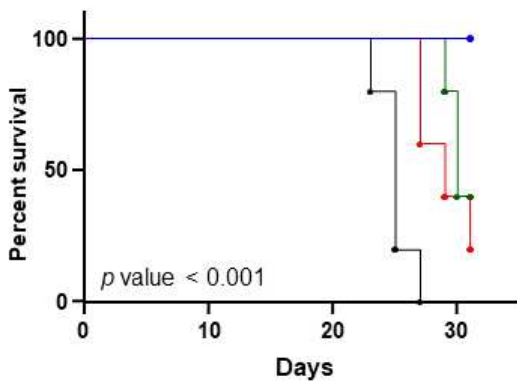


Figure 19. Anti-Tumor Effect of SVF SPH with DCs. a, The schedule of the test for the evaluation of anti-tumor effect. 5×10^4 of B16-OVA melanoma cells were subcutaneously injected to the right flank of the mice. The combinations of SVF-SPH or/and NP-OVA-loaded DCs were transplanted into kidney subcapsular space three times with a week intervals after tumor inoculation. b and c B16-OVA tumor growth. **** $p < 0.0001$ by Student's *t*-test. d, Survival curves of B16-OVA tumor bearing mice in a-c.

8. Discussion

Recently, multiple studies reported that tertiary lymphoid structures (TLS) improved the immunotherapy immune checkpoint blockade.^{63, 64} In particular, they said that B cells within the TLSs play a role for an effective T cell response. B cells within TLSs may act as antigen-presenting cells and induce the proliferation of tumor-associated T cell responses. B cells can also release various cytokines that activate and recruit effector cells such as T cells.⁶⁴ These studies didn't mention the role of stromal cells, but the interaction between stromal cells and B cells would be involved in generating TLSs via lymphotoxin signaling. In my study, DCs would play similar roles instead of B cells. Unlike well-organized secondary lymphoid organs, TLSs are formed after birth and have incomplete structures such as imperfect T and B cell segregation, a random mixture of T and B cells, or the absence of T cells or B cells.^{23,37} For the generation of lymphoid structures, $LT\beta R^+$ lymphoid tissue organizer cells (LTo) and $LT\beta R$ ligand⁺ lymphoid tissue inducer cells (LTi) are canonically necessary, initiating the recruitment of immune cells via lymphotoxin signaling.^{65,66} Therefore, the *in vivo* organogenesis including vessels and T cell clusters formed by DCs with SVFs (Fig. 8d, 12c) can be regarded as a kind of TLSs, and SVFs can be compared to “organizer” LTo-like cells and DCs to “inducer” LTi-like cells (Fig. 20a).

In addition to ordinary TLSs, several groups have attempted to create artificial lymphoid structures (ALS) for immunotherapy via the utilization of embryonic cells^{41,67} or genetically-modified

stromal cell lines.⁶⁸⁻⁷⁰ These studies showed marvelous insight, but they have limitations in that embryos or cell lines cannot be used in clinical trials. Alternatively, my results suggest that primary cells isolated from adipose tissue can complement these limitations through the easy method and mass-culture. My study is the first example of ALS formed by adult primary cells. In terms of keeping with the symmetry between immunostimulation and immunosuppression, my approach using primary fat-derived cells might also be appropriate for cell therapy more so than methods using genetically modified chemokine-overexpressing cell lines or administration of chemokines.

This study found that cultured SVFs can be a source of LN-like stromal cells including FRCs, LECs, and BECs. In particular, PDPN⁺ CD31⁻ FRC-like cells revealed that not only LT β R, PDGFR α , VCAM-1, and ICAM-1 (Fig. 5), but also Sca-1 and CD44 (data not shown) were expressed on the surface. Based on the phenotype, the FRC-like cells of cultured SVF seemed to be the most similar to FALC FRCs and splenic perivascular reticular cells.^{28, 71}

Several studies showed that SVFs were able to form new vessels via direct implantation of SVFs with the Matrigel forms⁵⁵ and spheroid culture using the magnetic levitation method.⁷² They observed that the implantation of SVF could induce the process of vascular network formation⁵⁵, and vessel-like structure formed by SVFs spheroid contained luminal layers with endothelial and perivascular stromal cells⁷², consistent with my data (Fig. 7-8).

Concerning enhanced anti-tumoral immune responses by SVFs with DCs, the proposed mechanism was illustrated in Fig. 20b

based on transcriptomic analysis and targeted protein analysis. Firstly, SVFs could recruit and activate DCs by expressing chemokines (CCL21 and *ccl19* in Fig. 6) and cytokines (Osteopontin in Fig. 10, *il6*, *tnf* in Fig. 15a), respectively. SVFs might also enhance DC survival via Osteopontin (Fig. 10, 16b). Thereafter, co-culturing SVFs with DCs revealed that the upregulated costimulatory molecules (CD40, CD80, DC-SIGN) and MHC II were observed (Fig. 16) and might activate T cells with the increased expression of cytokines (*il1a*, *il1b*, *il6*, *il12a* in Fig. 15b). Additionally, elevated chemokines including *ccl3*, *ccl4*, *ccl17*, *ccl20*, and *cxcl12* might be involved in the recruitment of T cells, confirmed by co-culturing SVF with DCs (Fig. 15b). Moreover, SVFs can recruit T cells by expressing chemokines (CCL21 and *ccl19* in *fig.6*, *ccl20*, *ccl22*, *cxcl10*, *cxcl16* in Fig. 15a), and SVF can support T cells through the cytokines (*il6*, *il12b*, *tnf* in Fig. 15a), costimulatory molecules (*cd40*, *icosl* in Fig. 15a), and survival factor, *il7* (Fig. 15a). Finally, recruited DC and T cells might be settled by adhesion molecules (e.g. ICAM-1, PDPN, PECAM-1, VCAM-1 in Fig. 4, 5, 15a) on the surface of SVFs. Besides, vessel-like structures generated by SVF SPHs might be explained by elevated cytokines related to vascularization (*vegfa*, *vegfc*, *pdgfb* in Fig. 15a). Through vessels, effector T cells might systemically migrate and enhance antigen-specific T cell responses (Fig. 20a). Notably, consistent with my data, transplantation of activated DCs with LN stromal cells in the collagen sponge into the renal subcapsular space significantly recruited T cells compared to transplantation of LN stromal cells alone in the collagen sponge⁷³, suggesting that SVFs are phenotypically and

functionally similar with LN stromal cells.

The *in vitro* experiments and analysis in my study could not perfectly reflect on all *in vivo* results, since co-culturing SVFs with DCs *in vitro* was performed for only 24 h, while *in vivo* renal subcapsular transplantation was observed after 2 weeks. However, T cell recruitment by SVF SPH with DCs and increased DC-based immune response were distinctly and reproducibly observed. Therefore, the kinetics analysis of *in vivo* organogenesis will be needed for further studies. For application to cell therapy, it might be necessary for human SVFs to be elucidated and easier administration of SVFs and DCs to be found instead of kidney subcapsular transplantation. Additionally, it is expected that SVFs can be used for a comparison study to the LN stromal cell and for an application to restore the structure and functions of impaired or aged LNs, based on the characteristics of SVFs in this article.

In conclusion, DC-based immune responses have been limited due to scarce migration/antigen delivery to draining LN and immunosuppressive TME. To solve these limitations, this study strategically applied the generation of *in situ* immune clusters by utilizing the resident DCs in the injection site to avoid TME and to fully exploit the entire potential of DCs-based therapy. Mimicking the mechanism of the immune responses in lymphoid tissues, lymphoid stroma-like 'cultured SVFs' were applied to support resident DCs as an alternative of LN stromal cells. As a result, it was observed that the administration of DCs with SVF SPHs enhanced antigen-specific T cell response as much as 2-fold higher than the DC alone-treated group and was able to improve the tumor-suppressing ability and survival rate. SVFs

from adipose tissue can be the source of LN stromal cells and could be beneficial for solving the limitations of DC-based immunotherapy, mimicking the way that LN stromal cells are involved in the immune response in lymphoid organs. In addition, this study provides the information that SVFs have the potential for clinical trials since SVFs can be isolated from self-fat tissues.

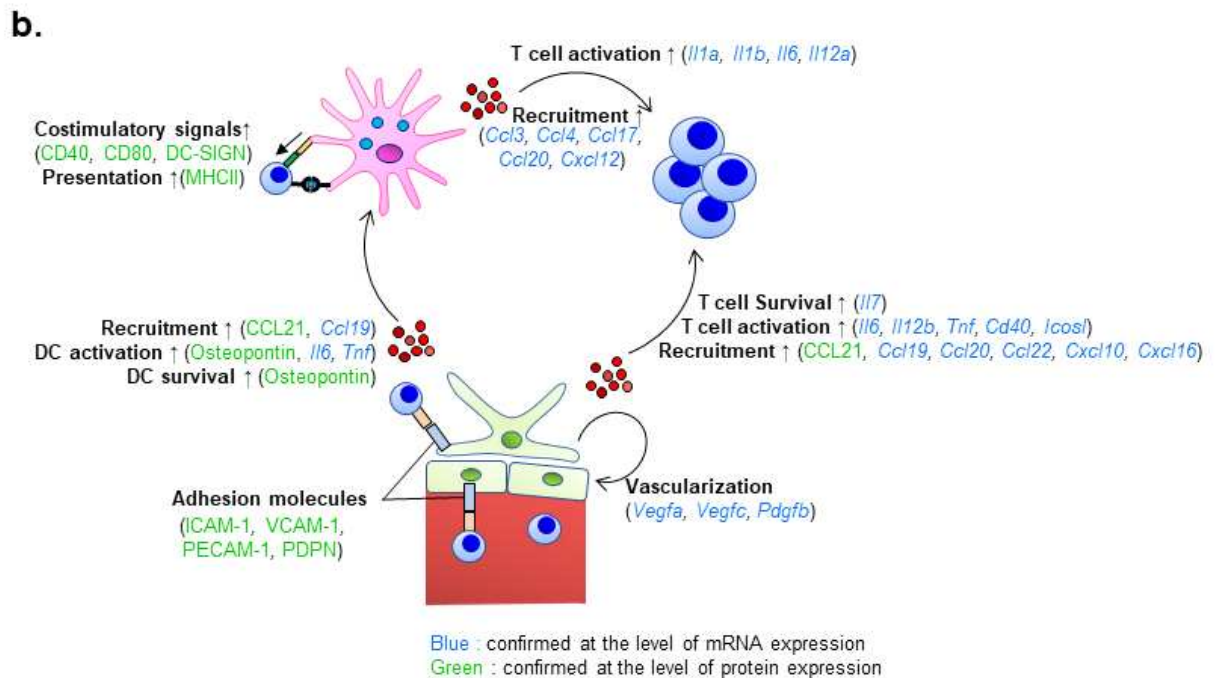
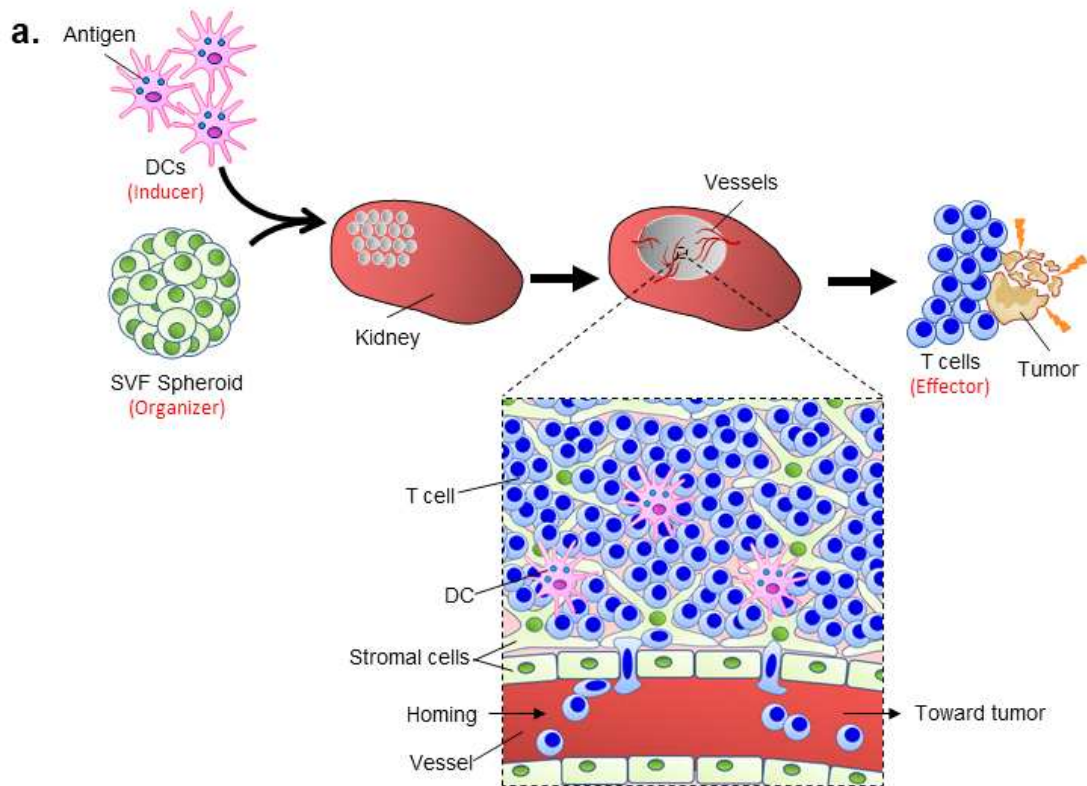


Figure 20. Summary and Proposed Mechanism. a. Illustrated summary of anti-tumoral results with *in situ* immune cluster by SVF spheroid with antigen-loaded DCs in the kidney subcapsule. SVFs can act as an ‘organizers’ of T cell clusters and SVFs interact with ‘inducers’, dendritic cells (DC), resulting in recruitment of T cells as ‘effectors’. T_{eff} cells spread to systemic immunity through vessels from SVFs. b. Proposed mechanism based on transcriptomic analysis and the expression of proteins. DCs and SVFs can attract and activate T cells via the expression of chemokines respectively indicated (green: confirmed at the level of protein expression, blue: confirmed at the level of mRNA expression). The level of co-stimulatory molecules on the DCs was upregulated. SVFs can attract and activate DCs via indicated factors. SVFs enhance survival of DCs and T cells expressing osteopontin and *il7*, respectively. The expression of adhesion molecules on the SVFs affects T cell migration and compels T cells to reside on site. The expression of genes such as *vegfa*, *vegfc* and *pdgfb* can induce the vascularization in way of autocrine.

9. References

1. Banchereau, J. & Steinman, R.M.J.N. Dendritic cells and the control of immunity. **392**, 245–252 (1998).
2. Mellman, I. & Steinman, R.M.J.C. Dendritic cells: specialized and regulated antigen processing machines. **106**, 255–258 (2001).
3. Wculek, S.K. et al. Dendritic cells in cancer immunology and immunotherapy. *Nat Rev Immunol* **20**, 7–24 (2020).
4. Gardner, A. & Ruffell, B. Dendritic Cells and Cancer Immunity. *Trends Immunol* **37**, 855–865 (2016).
5. Palucka, K. & Banchereau, J. Dendritic–cell–based therapeutic cancer vaccines. *Immunity* **39**, 38–48 (2013).
6. Sancho, D. et al. Tumor therapy in mice via antigen targeting to a novel, DC–restricted C–type lectin. **118**, 2098–2110 (2008).
7. Schetters, S.T. et al. Mouse DC–SIGN/CD209a as target for antigen delivery and adaptive immunity. **9**, 990 (2018).
8. Meixlsperger, S. et al. CD141⁺ dendritic cells produce prominent amounts of IFN– α after dsRNA recognition and can be targeted via DEC–205 in humanized mice. **121**, 5034–5044 (2013).
9. Schlitzer, A. et al. IRF4 transcription factor–dependent CD11b⁺ dendritic cells in human and mouse control mucosal IL–17 cytokine responses. **38**, 970–983 (2013).
10. Ruffell, B. et al. Macrophage IL–10 blocks CD8⁺ T cell–dependent responses to chemotherapy by suppressing IL–12 expression in intratumoral dendritic cells. **26**,

- 623–637 (2014).
11. Martínez-López, M., Iborra, S., Conde-Garrosa, R. & Sancho, D.J.E.j.o.i. Batf3-dependent CD103⁺ dendritic cells are major producers of IL-12 that drive local Th1 immunity against *Leishmania major* infection in mice. **45**, 119–129 (2015).
 12. Hildner, K. et al. Batf3 deficiency reveals a critical role for CD8 α ⁺ dendritic cells in cytotoxic T cell immunity. **322**, 1097–1100 (2008).
 13. Wculek, S.K. et al. Effective cancer immunotherapy by natural mouse conventional type-1 dendritic cells bearing dead tumor antigen. **7**, 100 (2019).
 14. Spranger, S., Dai, D., Horton, B. & Gajewski, T.F.J.C.c. Tumor-residing Batf3 dendritic cells are required for effector T cell trafficking and adoptive T cell therapy. **31**, 711–723. e714 (2017).
 15. Santos, P.M. & Butterfield, L.H.J.T.J.o.I. Dendritic cell-based cancer vaccines. **200**, 443–449 (2018).
 16. Bol, K.F., Schreiber, G., Gerritsen, W.R., de Vries, I.J. & Figdor, C.G. Dendritic Cell-Based Immunotherapy: State of the Art and Beyond. *Clin Cancer Res* **22**, 1897–1906 (2016).
 17. Cintolo, J.A., Datta, J., Mathew, S.J. & Czerniecki, B.J.J.F.o. Dendritic cell-based vaccines: barriers and opportunities. **8**, 1273–1299 (2012).
 18. Garg, A.D., Coulie, P.G., Van den Eynde, B.J. & Agostinis, P.J.T.i.i. Integrating next-generation dendritic cell vaccines into the current cancer immunotherapy landscape. **38**, 577–593 (2017).

19. Celli, S. et al. How many dendritic cells are required to initiate a T-cell response? **120**, 3945–3948 (2012).
20. Sabado, R.L., Balan, S. & Bhardwaj, N. Dendritic cell-based immunotherapy. *Cell Res* **27**, 74–95 (2017).
21. Acton, S.E. et al. Podoplanin-rich stromal networks induce dendritic cell motility via activation of the C-type lectin receptor CLEC-2. *Immunity* **37**, 276–289 (2012).
22. de Vries, I.J.M. et al. Effective migration of antigen-pulsed dendritic cells to lymph nodes in melanoma patients is determined by their maturation state. **63**, 12–17 (2003).
23. Gajewski, T.F., Schreiber, H. & Fu, Y.X. Innate and adaptive immune cells in the tumor microenvironment. *Nat Immunol* **14**, 1014–1022 (2013).
24. Quail, D.F. & Joyce, J.A. Microenvironmental regulation of tumor progression and metastasis. *Nat Med* **19**, 1423–1437 (2013).
25. Maman, S. & Witz, I.P. A history of exploring cancer in context. *Nat Rev Cancer* **18**, 359–376 (2018).
26. Riedel, A., Shorthouse, D., Haas, L., Hall, B.A. & Shields, J. Tumor-induced stromal reprogramming drives lymph node transformation. *Nat Immunol* **17**, 1118–1127 (2016).
27. Angela Riedel, J.S., David Shorthouse, Lisa Haas¹, Tim Young, Ana S H Costa, Sarah Davidson, Luisa Pedro, Thordur Oskarsson, Benjamin A Hall, Christian Frezza, Jacqueline Shields Tumor pre-conditioning of draining lymph node stroma by lactic acid. *bioRxiv* (2018).
28. Perez-Shibayama, C., Gil-Cruz, C. & Ludewig, B. Fibroblastic reticular cells at the nexus of innate and

- adaptive immune responses. *Immunol Rev* **289**, 31–41 (2019).
29. Buechler, M.B. & Turley, S.J. in *Seminars in immunology*, Vol. 35 48–58 (Elsevier, 2018).
 30. Fletcher, A.L., Acton, S.E. & Knoblich, K. Lymph node fibroblastic reticular cells in health and disease. *Nat Rev Immunol* **15**, 350–361 (2015).
 31. Mueller, S.N. & Germain, R.N. Stromal cell contributions to the homeostasis and functionality of the immune system. *Nat Rev Immunol* **9**, 618–629 (2009).
 32. Link, A. et al. Fibroblastic reticular cells in lymph nodes regulate the homeostasis of naive T cells. **8**, 1255–1265 (2007).
 33. Krishnamurthy, A.T. & Turley, S.J. Lymph node stromal cells: cartographers of the immune system. *Nat Immunol* **21**, 369–380 (2020).
 34. Brown, F.D. et al. Fibroblastic reticular cells enhance T cell metabolism and survival via epigenetic remodeling. **20**, 1668–1680 (2019).
 35. Turley, S.J., Fletcher, A.L. & Elpek, K.G. The stromal and haematopoietic antigen-presenting cells that reside in secondary lymphoid organs. *Nat Rev Immunol* **10**, 813–825 (2010).
 36. Angeli, V. & Yeo, P.K.J.F.i.i. Bi-directional crosstalk between lymphatic endothelial cell and T cell and its implications in tumor immunity. **8**, 83 (2017).
 37. Saxena, V. et al. Role of lymph node stroma and microenvironment in T cell tolerance. (2019).
 38. Malhotra, D. et al. Transcriptional profiling of stroma from

- inflamed and resting lymph nodes defines immunological hallmarks. *Nat Immunol* **13**, 499–510 (2012).
39. Acton, S.E. & Reis e Sousa, C.J.I.r. Dendritic cells in remodeling of lymph nodes during immune responses. **271**, 221–229 (2016).
 40. Benezech, C. et al. Lymphotoxin–beta receptor signaling through NF–kappaB2–RelB pathway reprograms adipocyte precursors as lymph node stromal cells. *Immunity* **37**, 721–734 (2012).
 41. Sitnik, K.M. et al. Context–Dependent Development of Lymphoid Stroma from Adult CD34(+) Adventitial Progenitors. *Cell Rep* **14**, 2375–2388 (2016).
 42. Meza–Perez, S. & Randall, T.D. Immunological Functions of the Omentum. *Trends Immunol* **38**, 526–536 (2017).
 43. Benezech, C. et al. Inflammation–induced formation of fat–associated lymphoid clusters. *Nat Immunol* **16**, 819–828 (2015).
 44. Bora, P., Majumdar, A.S.J.S.c.r. & therapy Adipose tissue–derived stromal vascular fraction in regenerative medicine: a brief review on biology and translation. **8**, 145 (2017).
 45. Bourin, P. et al. Stromal cells from the adipose tissue–derived stromal vascular fraction and culture expanded adipose tissue–derived stromal/stem cells: a joint statement of the International Federation for Adipose Therapeutics and Science (IFATS) and the International Society for Cellular Therapy (ISCT). *Cytotherapy* **15**, 641–648 (2013).
 46. Cho, N.–H. et al. A multifunctional core–shell nanoparticle

- for dendritic cell-based cancer immunotherapy. *Nature nanotechnology* **6**, 675 (2011).
47. Liu, H., Wu, J., Min, J.H., Zhang, X. & Kim, Y.K. Tunable synthesis and multifunctionalities of Fe₃O₄-ZnO hybrid core-shell nanocrystals. *Materials Research Bulletin* **48**, 551–558 (2013).
 48. Tolia, N.H. & Joshua-Tor, L. Strategies for protein coexpression in *Escherichia coli*. *Nature methods* **3**, 55–64 (2006).
 49. Kreiling, J.L., Brader, K., Kolar, C. & Borgstahl, G.E. A real-time and hands-on research course in protein purification and characterization: Purification and crystal growth of human inosine triphosphate pyrophosphatase. *Biochemistry and Molecular Biology Education* **39**, 28–37 (2011).
 50. Cavallaro, A.S., Mahony, D., Commins, M., Mahony, T.J. & Mitter, N. Endotoxin-free purification for the isolation of Bovine Viral Diarrhoea Virus E2 protein from insoluble inclusion body aggregates. *Microbial cell factories* **10**, 57 (2011).
 51. Cho, N.H. et al. A multifunctional core-shell nanoparticle for dendritic cell-based cancer immunotherapy. *Nat Nanotechnol* **6**, 675–682 (2011).
 52. Chung, H. et al. High mobility group box 1 secretion blockade results in the reduction of early pancreatic islet graft loss. **514**, 1081–1086 (2019).
 53. Trapnell, C., Pachter, L. & Salzberg, S.L.J.B. TopHat: discovering splice junctions with RNA-Seq. **25**, 1105–1111 (2009).

54. Fischer, A.H., Jacobson, K.A., Rose, J. & Zeller, R. Hematoxylin and eosin staining of tissue and cell sections. *CSH Protoc* 2008, pdb prot4986 (2008).
55. Koh, Y.J. et al. Stromal Vascular Fraction From Adipose Tissue Forms Profound Vascular Network Through the Dynamic Reassembly of Blood Endothelial Cells. *Arterioscl Throm Vas* 31, 1141–U1539 (2011).
56. Kessenbrock, K., Plaks, V. & Werb, Z. Matrix metalloproteinases: regulators of the tumor microenvironment. *Cell* 141, 52–67 (2010).
57. Nabeshima, K., Inoue, T., Shimao, Y. & Sameshima, T. Matrix metalloproteinases in tumor invasion: role for cell migration. *Pathology international* 52, 255–264 (2002).
58. Kawamura, K. et al. Differentiation, maturation, and survival of dendritic cells by osteopontin regulation. 12, 206–212 (2005).
59. Schulz, O., Hammerschmidt, S.I., Moschovakis, G.L. & Förster, R.J.A.r.o.i. Chemokines and chemokine receptors in lymphoid tissue dynamics. 34, 203–242 (2016).
60. Lukacs–Kornek, V. et al. Regulated release of nitric oxide by nonhematopoietic stroma controls expansion of the activated T cell pool in lymph nodes. 12, 1096–1104 (2011).
61. Hoch, R.V. & Soriano, P.J.D. Roles of PDGF in animal development. 130, 4769–4784 (2003).
62. Bai, Y., Bai, L., Zhou, J., Chen, H. & Zhang, L.J.C.i. Sequential delivery of VEGF, FGF–2 and PDGF from the polymeric system enhance HUVECs angiogenesis in vitro and CAM angiogenesis. 323, 19–32 (2018).

63. Cabrita, R. et al. Tertiary lymphoid structures improve immunotherapy and survival in melanoma. 1–5 (2020).
64. Helmink, B.A. et al. B cells and tertiary lymphoid structures promote immunotherapy response. 1–7 (2020).
65. Dieu-Nosjean, M.C. et al. Tertiary lymphoid structures, drivers of the anti-tumor responses in human cancers. **271**, 260–275 (2016).
66. Eckert, N., Permyer, M., Yu, K., Werth, K. & Förster, R.J.I.r. Chemokines and other mediators in the development and functional organization of lymph nodes. **289**, 62–83 (2019).
67. Cupedo, T., Jansen, W., Kraal, G. & Mebius, R.E.J.I. Induction of secondary and tertiary lymphoid structures in the skin. **21**, 655–667 (2004).
68. Suematsu, S. & Watanabe, T.J.N.b. Generation of a synthetic lymphoid tissue-like organoid in mice. **22**, 1539–1545 (2004).
69. Okamoto, N., Chihara, R., Shimizu, C., Nishimoto, S. & Watanabe, T.J.T.J.o.c.i. Artificial lymph nodes induce potent secondary immune responses in naive and immunodeficient mice. **117**, 997–1007 (2007).
70. Zhu, G. et al. Induction of tertiary lymphoid structures with antitumor function by a lymph node–derived stromal cell line. **9**, 1609 (2018).
71. Perez–Shibayama, C. et al. Fibroblastic reticular cells initiate immune responses in visceral adipose tissues and secure peritoneal immunity. **3**, eaar4539 (2018).
72. Daquinag, A.C., Souza, G.R. & Kolonin, M.G. Adipose tissue engineering in three–dimensional levitation tissue

culture system based on magnetic nanoparticles. *Tissue Engineering Part C: Methods* **19**, 336–344 (2013).

73. Komori, S. et al. SIRP α^+ dendritic cells promote the development of fibroblastic reticular cells in murine peripheral lymph nodes. **49**, 1364–1371 (2019).

국문 초록

서론: 수지상세포는 가장 강력한 항원 제시 세포이다. 수지상세포는 종양이나 병원체로부터 항원을 획득하여 림프절의 미접촉 T 세포에 항원을 전달하여 적응면역을 시작할 수 있도록 한다. 수지상세포의 이런 능력 덕분에 수지상세포 항암면역치료제가 개발되었지만 기대했던 것보다 임상시험 결과는 좋지 않았다. 본 연구에서는 수지상세포 매개 면역 반응을 향상시키기 위해서 지방 조직에서 추출한 기질세포를 수지상세포의 활성을 높일 수 있는 구조적 프레임으로 활용하였다.

방법: 지방 조직 유래 기질 세포를 얻기 위하여 내장 지방과 피하 지방 으로부터 기질혈관분획을 분리·배양하였다. 6~10일 동안 배양한 후, 스페로이드 배양 용기에 넣고 배양하여 기질혈관분획세포로 구성된 스페로이드를 생성하였다. 단일 세포 형태와 스페로이드 형태의 유전자 발현 차이를 측정하기 위하여 qPCR과 RNA 시퀀싱 분석이 수행되었다. 수지상세포는 Rag2 결손 마우스에서 골수를 분리한 후, 6일 이상 배양하여 얻을 수 있었다. 수지상세포는 LPS를 처리하여 활성화시키고 실험에 사용하였다. 항원 전달을 위해 산화철-산화아연 나노입자에 산화아연에 결합하는 펩티드가 붙어있는 난백알부민 입자를 결합시킨 후, 수지상세포에 처리하였다. 스페로이드 형태의 기질혈관분획과 수지상세포에 의해 생체 내에서 형성되는 구조를 알아보기 위해 신장막 안에 이식하였다. 생체 내 구조는 공초점 형광 이미징 기술과 H&E 염색으로 분석하였다. 기질혈관분획과 수지상세포의 상호작용은 함께 배양하여 측정하였다. 항원 특이적 면역반응 측정을 위해 기질혈관분획 스페로이드와 수지상세포를 마우스에 면역하였고 OVA-특이적 구조적 결합성 복합체 테트라머를

사용하여 염색한 후 유세포 분석기로 분석하였다. 기질혈관분획과 수지상세포의 항암효능을 검증하기 위하여 B16MO5 종양세포를 마우스 옆구리에 주입한 후 1주일 간격으로 총 3번 면역하였고, 종양의 크기와 생존율을 측정하였다.

결과: 배양된 기질혈관분획은 표현 형질과 기능이 림프절 기질세포와 유사한 세포들로 구성되어 있다는 사실을 확인하였다. 기질혈관분획 스페로이드는 혈관과 유사한 구조를 생체 내·외에서 형성하였다. 또한, 기질혈관분획 스페로이드는 면역세포를 불러오는 케모카인들을 발현하는 것을 확인하였고, 생체 외 실험에서 수지상세포의 이동을 촉진하는 것으로 확인되었다. 또한 기질혈관분획과 함께 배양한 성숙 수지상세포의 활성화 정도와 분열능력, 생존능이 증가했음을 확인하였다. 기질혈관분획 스페로이드와 수지상세포를 신장막에 이식한 결과, 2주 후 주입한 자리에 대조군보다 훨씬 많은 숫자의 T 세포가 모여 있는 것을 확인하였다. 기질혈관분획 스페로이드와 항원을 탑재한 수지상세포를 면역한 마우스에서 기질혈관분획 스페로이드만 면역하거나 수지상세포만 면역한 마우스보다 항원 특이적 T 세포 면역반응이 향상되어 있음이 관찰되었다. 게다가, 기질혈관분획 스페로이드와 수지상세포를 주입한 마우스에서는 종양에 대한 항암 효과가 대조군에 비해 유의하게 향상되어 있음을 알 수 있었다.

결론: 종합해 볼 때, 배양한 기질혈관분획은 림프절 기질세포와 유사한 세포를 만드는데 사용될 수 있고, 수지상세포의 활성을 증가시킬 수 있다. 이는 기질혈관분획이 수지상세포 면역치료의 항원 특이적 면역 반응을 증가시키고, 종양에 대한 항암효과를 향상시키는 것을 통해 확인할

수 있었다. 그러므로 본 연구는 지방 조직에서 분리한 기질혈관분획을 활용하여 수지상세포 매개의 면역 반응을 향상시킬 수 있는 새로운 방법을 제시하였다.

주요어: 기질혈관분획, 수지상세포, 면역치료, 3차 림프 구조, 림프절 기질세포

학번: 2014-25071